Article

Cell Reports

Lymph Node Stromal Cells Generate Antigen-Specific Regulatory T Cells and Control Autoreactive T and B Cell Responses

Graphical Abstract

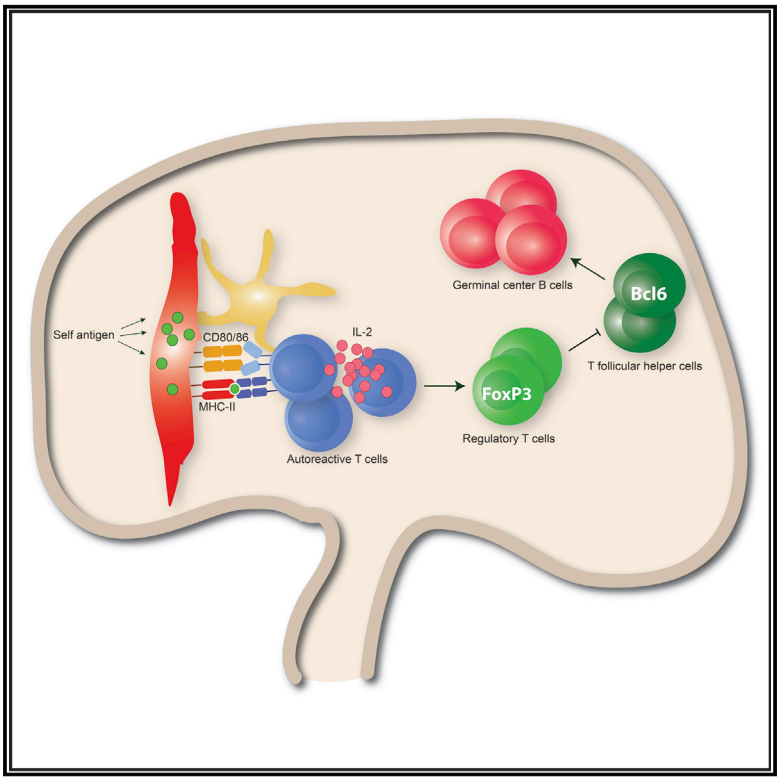

Authors

Reza Nadafi, Catarina Gago de Graça, Eelco D. Keuning, ..., Rogier M. Reijmers, Lisa G.M. van Baarsen, Reina E. Mebius

Correspondence

r.mebius@amsterdamumc.nl

In Brief

Lymph node stromal cells influence adaptive immune cells in various ways. Nadafi et al. show that by presenting self-antigens on MHC class II, lymph node stromal cells promote the differentiation of $CD4^+$ T cells into regulatory T cells, which are able to prevent the generation of follicular T helper cells and germinal center B cells directed against the same self-antigen.

Highlights

- Lymph node stromal cells convert naive $CD4^+$ T cells into T_{REG} cells
- Conversion of T_{REG} cells by lymph node stromal cells is IL-2 dependent
- Autoreactive T_{FH} cells and B cells are controlled by lymph node stromal cells

Nadafi et al., 2020, Cell Reports *30*, 4110–4123
March 24, 2020
https://doi.org/10.1016/j.celrep.2020.03.007

CellPress

OPEN ACCESS
CellPress

Cell Reports
Article

Lymph Node Stromal Cells Generate Antigen-Specific Regulatory T Cells and Control Autoreactive T and B Cell Responses

Reza Nadafi,[1,2] Catarina Gago de Graça,[1] Eelco D. Keuning,[1] Jasper J. Koning,[1] Sander de Kivit,[2,3] Tanja Konijn,[1] Sandrine Henri,[4] Jannie Borst,[2,3] Rogier M. Reijmers,[1,7] Lisa G.M. van Baarsen,[5,6] and Reina E. Mebius[1,8,*]

[1]Department of Molecular Cell Biology and Immunology, Amsterdam UMC, Vrije Universiteit Amsterdam, Amsterdam Infection and Immunity Institute, Amsterdam, the Netherlands
[2]Department of Immunohematology and Blood Transfusion, Leiden University Medical Center, Leiden, the Netherlands
[3]Oncode Institute, Leiden University Medical Center, Leiden, the Netherlands
[4]Centre d'Immunologie de Marseille-Luminy, Aix Marseille Universite, INSERM, CNRS, 13288 Marseille, France
[5]Department of Rheumatology and Clinical Immunology and Department of Experimental Immunology, Amsterdam Infection and Immunity Institute, Amsterdam UMC and University of Amsterdam, Amsterdam, the Netherlands
[6]Amsterdam Rheumatology and Immunology Center (ARC), Academic Medical Center, Amsterdam, the Netherlands
[7]Present address: LUMICKS, Pilotenstraat 41, Amsterdam, the Netherlands
[8]Lead Contact
*Correspondence: r.mebius@amsterdamumc.nl
https://doi.org/10.1016/j.celrep.2020.03.007

SUMMARY

Within lymph nodes (LNs), T follicular helper (T_{FH}) cells help B cells to produce antibodies, which can either be protective or autoreactive. Here, we demonstrate that murine LN stromal cells (LNSCs) suppress the formation of autoreactive T_{FH} cells in an antigen-specific manner, thereby significantly reducing germinal center B cell responses directed against the same self-antigen. Mechanistically, LNSCs express and present self-antigens in major histocompatibility complex (MHC) class II, leading to the conversion of naive $CD4^+$ T cells into T regulatory (T_{REG}) cells in an interleukin-2 (IL-2)-dependent manner. Upon blockade of T_{REG} cells, using neutralizing IL-2 antibodies, autoreactive T_{FH} cells are allowed to develop. We conclude that the continuous presentation of self-antigens by LNSCs is critical to generate antigen-specific T_{REG} cells, thereby repressing the formation of T_{FH} cells and germinal center B cell responses. Our findings uncover the ability of LNSCs to suppress the early activation of autoreactive immune cells and maintain peripheral tolerance.

INTRODUCTION

Autoimmunity emerges when immune tolerance against self-antigens is lost. As a result, the recognition of self-antigens by cells of the adaptive immune system leads to the formation and development of autoreactive B cells in germinal centers (GCs) and autoantibody production (Yanaba et al., 2008). T follicular helper (T_{FH}) cells are speculated to be the central players in the pathogenesis of autoimmune diseases by steering a selective expansion of high-affinity autoreactive B cells in GCs (Craft, 2012). Accordingly, alterations in T_{FH} cells are associated with the development of a broad range of autoimmune diseases such as juvenile dermatomyositis (Morita et al., 2011), Sjogren's syndrome (Simpson et al., 2010; Szabo et al., 2013), systemic lupus erythematous (He et al., 2013; Simpson et al., 2010), and rheumatoid arthritis (Arroyo-Villa et al., 2014; Ma et al., 2012; Rao et al., 2017; Wang et al., 2013; Zhang et al., 2015). T_{FH} cells differentiate within the T cell area of lymph nodes (LNs) and are identified by the expression of Cxcr5, PD-1, and Bcl6 (Crotty, 2014). Bcl6 is an essential transcription factor for their development, while expression of chemokine receptor Cxcr5 guides T_{FH} cell migration to B cell follicles, where they contribute to the maturation and differentiation of B cells (Crotty, 2014).

Regulatory pathways need to be in place to control the formation and development of autoreactive T_{FH} cells. Among diverse regulatory mechanisms, it is particularly important to mention the fundamental role of T regulatory (T_{REG}) cells in preventing autoreactive T cell formation in the thymus and periphery (Josefowicz et al., 2012). Generation of T_{REG} cells in the thymus is the result of the recognition of self-antigens by T cells bearing a high-affinity T cell receptor (TCR) (Jordan et al., 2001). Expression of the vast majority of self-antigens in the thymus is restricted to a unique non-hematopoietic stromal cell population known as medullary thymic epithelial cells (mTECs), which are able to steer the differentiation of $CD4^+$ T cells with high-affinity TCRs into $FoxP3^+$ T_{REG} cells (Anderson et al., 2002; Aschenbrenner et al., 2007; Derbinski et al., 2001; Hinterberger et al., 2010). The expression and presentation of self-antigens, however, is not limited to mTECs in the thymus, as several LN stromal cell (LNSC) subsets— including fibroblastic reticular cells (FRCs), lymphatic endothelial cells (LECs), blood endothelial cells (BECs), and double-negative (DN) cells—also display unique expression patterns of self-antigens (Cohen et al., 2010; Fletcher et al., 2010; Nichols et al., 2007). The effect of self-antigen presentation by LNSCs on autoreactive T cells has been shown in various studies (Cohen et al., 2010; Dubrot et al., 2014; Fletcher et al., 2010; Lee et al., 2007; Magnusson et al., 2008; Nichols et al., 2007; Rouhani et al., 2015), suggesting that the process

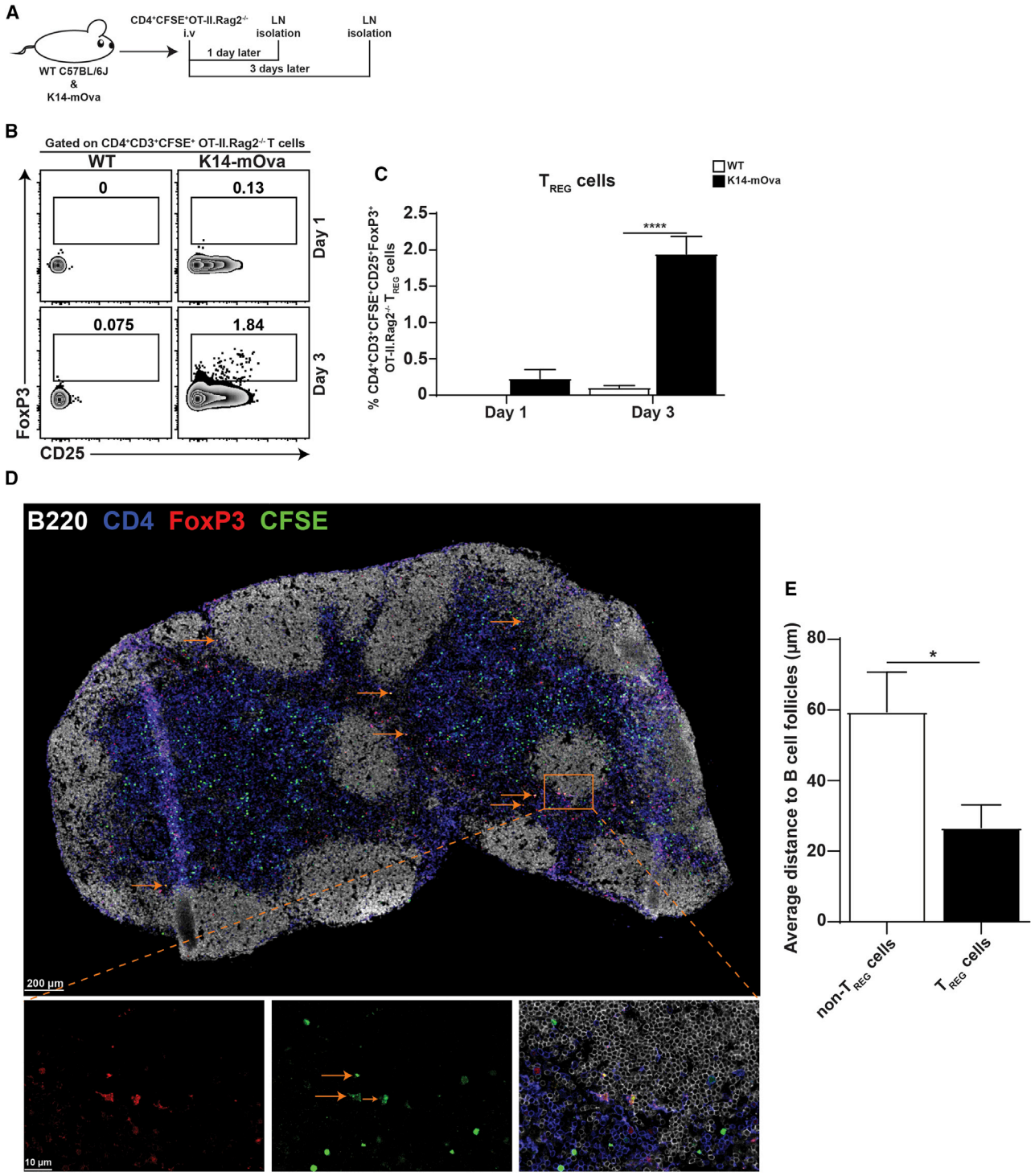

Figure 1. Antigen-Specific T_{REG} Cell Conversion Occurs in the Lymph Nodes

(A) *In vivo* experimental design to study T_{REG} cell conversion in LNs. WT C57L/6J and K14-mOva mice were intravenously injected with 5–8 × 10^6 CFSE-labeled $CD4^+$ OT-II.*Rag2*$^{-/-}$ T cells. 1 and 3 days after $CD4^+$ T cell transfer, mice were sacrificed, and LNs were isolated for analysis of transferred $CD4^+$ OT-II.*Rag2*$^{-/-}$ T cells by flow cytometry (B and C) and immunofluorescence (D and E).

(B) Representative contour plots of live CFSE-labeled $CD4^+CD3^+$ OT-II.*Rag2*$^{-/-}$ T cells in peripheral LNs, in which the numbers in the plots display the frequency of $CD25^+FoxP3^+$ T_{REG} cells.

(legend continued on next page)

of peripheral tolerance is necessary to further complete T_{REG} cell generation in the thymus.

Recently, we have demonstrated that LNSCs constrain immune reactivity via presentation of self-antigens in major histocompatibility complex (MHC) class II, which results in the selective maintenance of antigen-specific T_{REG} cells (Baptista et al., 2014). The expression of MHC class II by LNSCs and not dendritic cells (DCs) was shown to be critical to preventing the activation of both $CD4^+$ and $CD8^+$ cells (Baptista et al., 2014; Dubrot et al., 2018). Nevertheless, the question of whether self-antigen presentation by LNSCs may in fact induce antigen-specific T_{REG} cell formation, analogous to the function of non-hematopoietic stromal cells in the thymus, remains unsolved.

Using antigen-specific $CD4^+$ T cells from TCR transgenic mice, we showed, with *in vitro* and *in vivo* systems, that antigen presentation by LNSCs resulted in the conversion of naive $CD4^+$ T cells into antigen-specific $CD25^+FoxP3^+$ T_{REG} cells, a process that depended on interleukin-2 (IL-2). Converted T_{REG} cells were preferentially present in the area close to the B cell follicles. These T_{REG} cells were necessary for the LNSC-mediated suppression of autoreactive T_{FH} cells, which supported the generation of autoreactive GC B cells. Altogether, our data reveal that LNSCs critically participate in maintaining tolerance by expressing and presenting self-antigens necessary for the conversion of naive T cells into antigen-specific T_{REG} cells.

RESULTS

Naive $CD4^+$ T Cells Can Convert into T_{REG} Cells in the LNs

We have previously shown that under steady-state conditions, LNSCs are essential for the maintenance of antigen-specific T_{REG} cells via the presentation of self-antigens in MHC class II (Baptista et al., 2014). However, it is not clear whether self-antigen presentation by LNSCs leads to the induction of T_{REG} cells, or if it only provides survival signals to existing T_{REG} cells. To directly address this, we used K14-mOva transgenic mice, where membrane-bound ovalbumin (Ova) is expressed as a skin antigen by keratinocytes under the human keratin 14 promoter (Baptista et al., 2014; Bianchi et al., 2009). Notably, Ova mRNA is expressed by LNSCs and not by any other antigen-presenting cell such as B cells, macrophages, or DCs at steady state within the LN (Figure S1A). The expression of Ova as a skin self-antigen is at levels equivalent to those of Mlana and Tryosinase, two skin-restricted endogenous antigens previously shown to be expressed by LNSCs (Figure S1A) (Fletcher et al., 2010). This indicates that in K14-mOva LNs, stromal cells are the only cell type that express Ova as a self-antigen. To explore the contribution of LNSCs in T_{REG} cell conversion *in vivo*, naive carboxyfluorescein succinimidyl ester (CFSE)-labeled $CD4^+$ T cells from OT-II.*Rag2*$^{-/-}$, which lack endogenous thymic $CD25^+FoxP3^+$ T_{REG} cells (Figure S1B), were intravenously injected into wild-type (WT) C57BL/6J and K14-mOva mice. LNs were isolated 1 and 3 days after the CFSE-labeled $CD4^+$ T cell transfer (Figure 1A). Analysis of peripheral (axillary, brachial, inguinal, and popliteal) LNs at day 3 showed that Ova-specific TCR-transgenic $CD4^+CD3^+$ OT-II.*Rag2*$^{-/-}$ T cells converted into $CD25^+FoxP3^+$ T_{REG} cells solely in K14-mOva LNs, wherein Ova is exclusively expressed as a self-antigen by LNSCs. Conversion of $CD4^+$ T cells to T_{REG} cells required at least 3 days, as the conversion was not observed at day 1 of the $CD4^+$ T cells' transfer (Figures 1B and 1C). Furthermore, the frequency of endogenous $CD25^+FoxP3^+$ T_{REG} cells was comparable between WT and K14-mOva LNs (Figures S2A and S2B). To explore the location of converted T_{REG} in the LNs under homeostatic conditions, we injected CFSE-labeled $CD4^+$ T cells from OT-II.*Rag2*$^{-/-}$ to K14-mOva mice. Three days later, peripheral LNs were isolated, and LN sections were stained with a multiplexed antibody panel. Injected CFSE-labeled $CD4^+$ T cells from OT-II.*Rag2*$^{-/-}$ appeared to be broadly distributed throughout the LN (Figure 1D). Nevertheless, quantitative analysis revealed that converted T_{REG} cells were mainly concentrated at the follicle-T-zone interface and interfollicular regions close to the B cell area (Figures 1E and S2C). These data show that antigen-specific naive T cells can be converted into T_{REG} cells within LNs upon self-antigen encounter and that they preferentially localize in the T cell area close to the B cell follicles.

Antigen Presentation by LNSCs Results in the Conversion of Naive $CD4^+$ T Cells into Antigen-Specific T_{REG} Cells

To study the mechanism of T_{REG} cell conversion by LNSCs, co-cultures of Ova-expressing LNSC lines (isolated from K14-mOva mice) and Ova-specific TCR transgenic $CD4^+$ T cells from OT-II.*Rag2*$^{-/-}$ transgenic mice were started. In this *in vitro* model, Ova is expressed as a self-antigen by the K14-mOva LEC and FRC lines and is absent in the control cell lines, while all cell lines are devoid of hematopoietic antigen-presenting cells (Figures S3A and S3B). In these co-culture experiments, T cell activation could be observed by the upregulation of CD25 at 48 h of culture only when T cells were cultured together with K14-mOva LECs. Subsequently, by 72 h of culture, a distinct population of $CD25^+FoxP3^+$ T_{REG} cells was present, and the frequency of these cells further increased by 96 h of culture (Figures 2A–2C). This conversion into $FoxP3^+$ cells was not observed in the presence of the WT LEC line or in the absence of stromal cells (medium) (Figures 2A–2C). Similarly, the K14-mOva FRC line was

(C) Frequency of $CD25^+FoxP3^+$ T_{REG} cells within $CD4^+CD3^+CFSE^+$ OT-II.*Rag2*$^{-/-}$ T cells in peripheral LNs of WT and K14-mOva mice. The data represent the mean ± SEM for one (n = 4 mice per group for day 1) and two (n = 3 mice per group for day 3) independent experiments analyzed by two-way ANOVA followed by Turkey's multiple comparison test. ****$p < 0.0001$.

(D) Representative immunofluorescence staining of an entire brachial LN section from K14-mOva mice. Arrows point to representative converted T_{REG} cells. Images are representative of four LNs (inguinal, brachial, axillary, and popliteal) from a total of three mice. Three sections, representing three different locations within each LN, were analyzed.

(E) Bar graph representing the average distance of $CFSE^+CD4^+FoxP3^+$ T_{REG} cells to the B cell area. n = mean of 4 LNs/3 mice. Data analyzed by unpaired Student's t test. *$p < 0.05$.

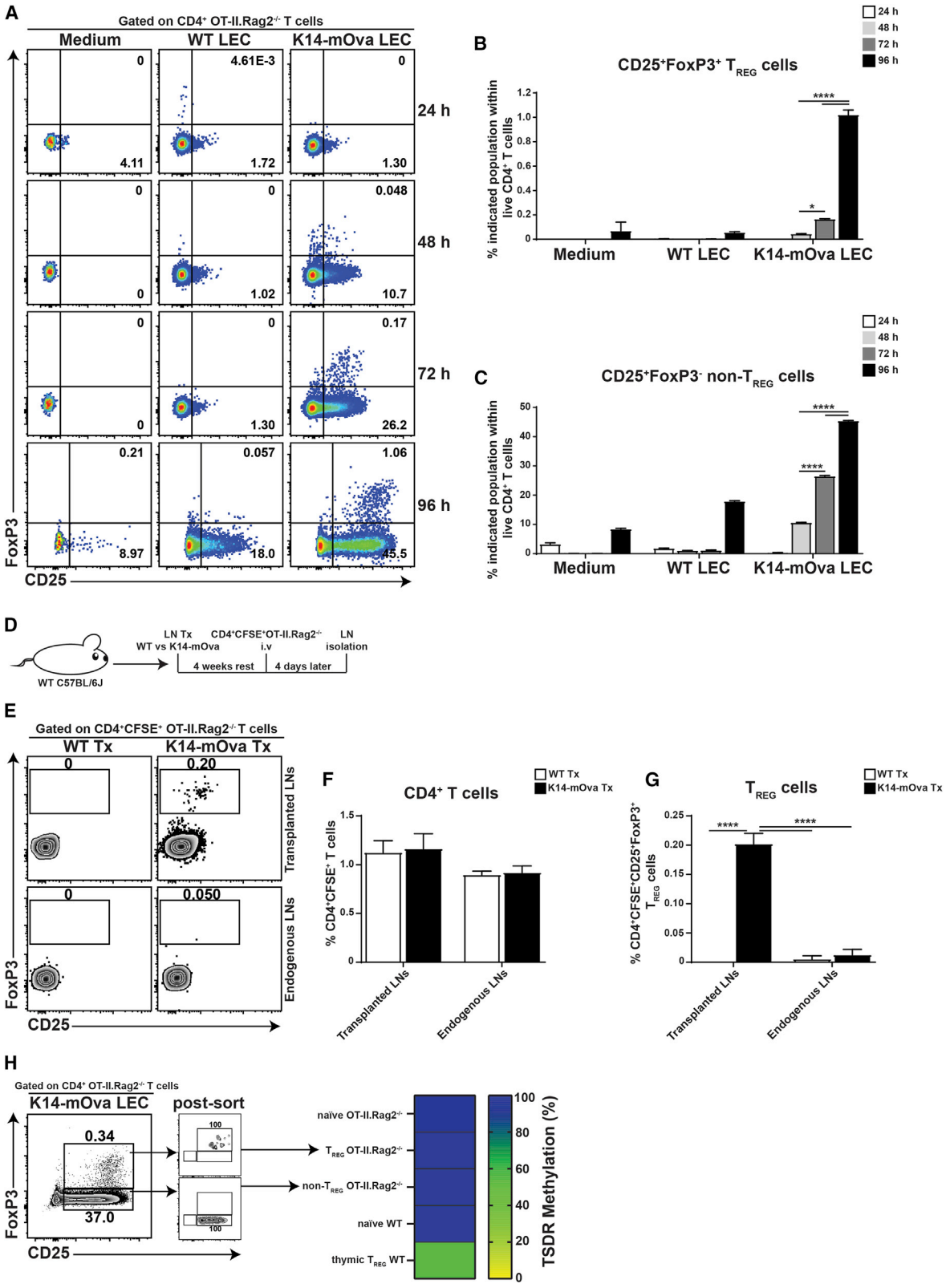

(legend on next page)

able to convert CD4$^+$ OT-II.*Rag2*$^{-/-}$ T cells into CD25$^+$FoxP3$^+$ T_{REG} cells. Hereto, we used early cell line passages, as FRCs tend to lose the expression of Ova upon long-term culture (Figures S3A–S3C). In order to determine whether the conversion of naive CD4$^+$ T cells toward T_{REG} cells was solely dependent on LNSCs, sorted naive CD4$^+$ OT-II.*Rag2*$^{-/-}$ T cells (99% pure) versus magnetic bead-enriched naive CD4$^+$ OT-II.*Rag2*$^{-/-}$ T cells were co-cultured with LNSCs for 3 days. These experiments showed that the presence of a minor impurity of DCs within the bead-enriched fraction of CD4$^+$ T cells was necessary for the conversion toward CD25$^+$FoxP3$^+$ T_{REG} cells, while these were absent within the sorted CD4$^+$ T cells (Figures S3D–S3H). In the absence of these DCs, CD25$^-$FoxP3$^+$ T_{REG} cells, which can still be classified as T_{REG} cells (Owen et al., 2019; Zelenay et al., 2005), were generated, while CD25$^+$FoxP3$^+$ T_{REG} cells were absent (Figures S3D–S3H). These data suggest that both FRCs and LECs can present self-antigens to naive CD4$^+$ T cells, which converted—with the assistance of DCs—into CD25$^+$FoxP3$^+$ T_{REG} cells upon antigen recognition. Although mRNA for the self-antigen Ova was only expressed by LNSCs (Figure S1A), skin-derived DCs could have picked up Ova in the skin and, as such, have contributed to antigen presentation in the LN. Therefore, to determine the potential contribution of LNSCs in T_{REG} cell conversion, we transplanted (Tx) K14-mOva LNs into WT hosts and analyzed the fate of the transferred naive CFSE-labeled CD4$^+$ OT-II.*Rag2*$^{-/-}$ T cells (Figure 2D). In our transplantation model, popliteal LNs of WT recipient mice were surgically removed and replaced by LNs from either WT (WT Tx) or K14-mOva (K14-mOva Tx) mice. After 4 weeks, lymphatic and blood vasculature are reconnected to the Tx LNs. While LNSCs within the transplant are of donor origin, nearly all immune cells of the donor animal are replaced by host-derived cells (Baptista et al., 2014; Hammerschmidt et al., 2008; Molenaar et al., 2009; Wolvers et al., 1999). Consequently, Ova expression as self-antigens is confined to the LNSCs within K14-mOva Tx LNs. Four days after the intravenous injection of naive CFSE-labeled CD4$^+$ OT-II.*Rag2*$^{-/-}$ T cells, both Tx and endogenous (host inguinal) LNs were analyzed. The frequency of CFSE$^+$CD4$^+$ T cells in transplanted and endogenous LNs was comparable between K14-mOva Tx LNs and WT Tx LNs. However, CFSE$^+$CD4$^+$ OT-II.*Rag2*$^{-/-}$ T cells converted into CD25$^+$FoxP3$^+$ T_{REG} cells when Ova was expressed as a self-antigen by LNSCs, as seen in K14-mOva Tx LNs (Figures 2E–2G). Further characterization of the converted CD25$^+$FoxP3$^+$ T_{REG} cells in K14-mOva Tx LNs showed a negligible expression of Cxcr5, a lack of PD-1, and a high expression of CD62L when compared to endogenous T_{FH} and T_{REG} cells (Figure S4A). Moreover, conversion of CD4$^+$ T cells was not observed in WT Tx LNs or endogenous LNs (Figures 2E–2G). There were no differences between the two groups in the frequencies of endogenous (host-derived) CD4$^+$ T cells and T_{REG} cells within the transplanted and the endogenous LNs (Figures S4B–S4D). In thymic T_{REG} cells, the T_{REG}-specific demethylated region (TSDR) in the *FoxP3* gene locus is significantly demethylated, which is required for stable FoxP3 expression (Baron et al., 2007; Floess et al., 2007). The TSDR of OT-II.*Rag2*$^{-/-}$ T_{REG} cells induced by LNSCs was methylated to the same degree as in activated non-T_{REG} cells of the OT-II.*Rag2*$^{-/-}$ and in contrast to the demethylated TSDR in thymic T_{REG} cells (Figure 2H). This result corroborated that the OT-II.*Rag2*$^{-/-}$ T_{REG} cells induced by LNSCs originated from the activated conventional OT-II.*Rag2*$^{-/-}$ T cells. Altogether, these data show that in steady state, the presentation of self-antigens by LNSCs leads to the conversion of naive CD4$^+$ T cells into CD25$^+$FoxP3$^+$ T_{REG} cells upon antigen recognition by the TCR.

T_{REG} Conversion by LNSCs Requires IL-2 and Co-stimulation

To assess the specific requirements for T_{REG} cell conversion by LNSCs, we addressed whether IL-2 was involved in this process, as IL-2 is crucial in T_{REG} cell maintenance and function (Abbas et al., 2018; Cheng et al., 2011; D'Cruz and Klein, 2005; Fontenot et al., 2005) and implicated in T_{REG} cell generation in the thymus (Malek et al., 2002). Hereto, neutralizing IL-2 antibody was added to the co-culture of naive Ova-specific TCR-transgenic CD4$^+$ T cells from OT-II.*Rag2*$^{-/-}$ with WT LEC or K14-mOva LEC lines. Blocking of IL-2 in the culture completely prevented the conversion of naive CD4$^+$ T cells into T_{REG} cells (Figures 3A–3C).

Figure 2. LNSCs Convert Antigen-Specific Naive CD4$^+$ T Cells into T_{REG} Cells

(A) CD4$^+$ T cells obtained from spleens and LNs of OT-II.*Rag2*$^{-/-}$ mice were either cultured alone (medium) (n = 2) or co-cultured with WT LEC (n = 2) or K14-mOva LEC (n = 2) stromal cell lines, and CD4$^+$ T cells were harvested at the indicated time points and analyzed by flow cytometry. Representative density plots are shown; the numbers in the plots correspond to the frequency of the cells within drawn gates of the live CD4$^+$ OT-II.*Rag2*$^{-/-}$ T cell population.

(B and C) Bar graphs represent the mean frequency of (B) CD25$^+$FoxP3$^+$ T_{REG} cells and (C) CD25$^+$FoxP3$^-$ non-T_{REG} cells. The graphs show mean ± SEM of triplicate co-cultures and are representative of two independent experiments (24 h, 48 h, and 72 h) and one independent experiment (96-h time point). Data analyzed by two-way ANOVA followed by Turkey's multiple comparison test. *$p < 0.05$; ****$p < 0.0001$.

(D) Experimental design to study T_{REG} cell conversion by LNSCs *in vivo*. LNs, either derived from WT or K14-mOVA mice, were transplanted into WT C57L/6J mice, and after 4 weeks of recovery, WT Tx and K14-mOva Tx mice were intravenously injected with 8×10^6 CFSE-labeled CD4$^+$ OT-II.*Rag2*$^{-/-}$ T cells. 4 days after CD4$^+$ T cell transfer, mice were sacrificed, and transferred CD4$^+$ OT-II.*Rag2*$^{-/-}$ T cells in both transplanted and endogenous (inguinal) LNs were examined using flow cytometry.

(E) Representative contour plots of live CFSE-labeled CD4$^+$ OT-II.*Rag2*$^{-/-}$ T cells within transplanted (top) and endogenous (bottom) LNs, in which the numbers in the plots display the frequency of CD25$^+$ FoxP3$^+$ T_{REG} cells.

(F and G) Frequency of CD4$^+$CFSE$^+$ OT-II.*Rag2*$^{-/-}$ T cells in endogenous and transplanted LNs (F) and frequency of CD25$^+$ FoxP3$^+$ T_{REG} cells within the live CFSE-labeled CD4$^+$ OT-II.*Rag2*$^{-/-}$ T cell population (G). The data represent the mean ± SEM; n = 5 mice per group and analyzed by two-way ANOVA followed by Turkey's multiple comparison test. ****$p < 0.0001$.

(H) CD4$^+$ T cells were obtained from spleens and LNs of OT-II.*Rag2*$^{-/-}$ mice and co-cultured with K14-mOva LEC lines. After 72 h, CD4$^+$ T cells were harvested, and converted T_{REG} cells and non-T_{REG} cells were sorted and compared to sorted naive OT-II.*Rag2*$^{-/-}$ (CD4$^+$CD3$^+$CD62L$^+$), sorted naive WT (CD4$^+$CD3$^+$CD62L$^+$), and sorted thymic T_{REG} WT (CD4$^+$CD3$^+$CD25^{hi}). Heatmap represents the percentage of T_{REG}-specific demethylated region (TSDR) DNA methylation per subset.

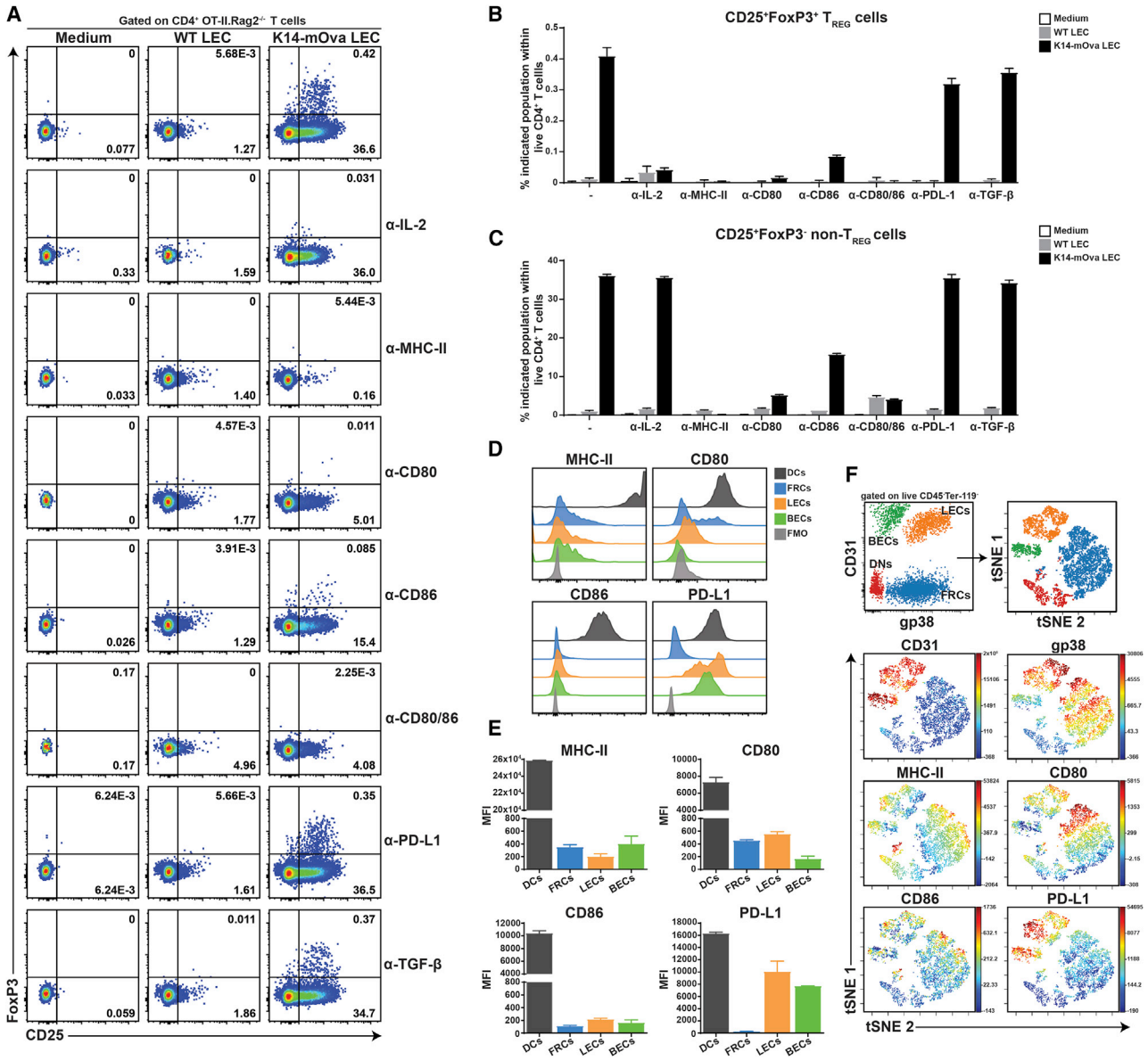

Figure 3. IL-2 and CD80/86 Are Necessary for T_{REG} Cell Conversion by LNSCs

(A) $CD4^+$ T cells were obtained from spleens and LNs of OT-II.*Rag2*$^{-/-}$ mice and either cultured alone (medium) (n > 4) or co-incubated with WT LEC (n = 2 for all conditions) or K14-mOva LEC stromal cell lines in the presence or absence of neutralizing antibodies, as indicated in the figure (n > 4 for anti-IL-2, anti-MHC class II; n = 2 for anti-CD80, anti-CD86, anti-CD80/CD86, anti-PD-L1, anti-TGF-β). After 72 h, $CD4^+$ T cells were harvested and analyzed by flow cytometry. Representative density plots are shown. The numbers in the plots represent the frequency of the cells within the quadrants of the live $CD4^+$ OT-II.*Rag2*$^{-/-}$ T cell population.

(B and C) Bar graphs represent the mean frequency of (B) $CD25^+FoxP3^+$ T_{REG} cells and (C) $CD25^+$ $FoxP3^-$ non-T_{REG} cells. The graphs show mean ± SEM of triplicate co-cultures and are representative of two independent experiments.

(D) Peripheral LNs from WT C57BL/6J mice were isolated and digested and stained for CD45, Ter-119, CD31, and gp38. Stromal cells were gated as $CD45^-$Ter-119^- cells, and the expression of co-stimulatory and inhibitory molecules on different subclasses of LNSCs, as defined by CD31 and gp38 expression, were assessed using flow cytometry. Histograms show the expression of indicated receptors on different stromal cell subsets in comparison to DCs ($CD45^+CD11c^+$).

(E) Mean fluorescence intensity (MFI) of MHC class II, CD80,CD86, and PD-L1 on LNSC subsets and DCs ($CD45^+CD11c^+$). The graphs depict the mean ± SEM (n = 3 mice per experiment) and are representative of three independent experiments.

(F) Data are shown as tSNE plots overlaid with the expression of selected markers.

Similarly, blockage of MHC class II also prevented T_{REG} cell conversion (Figures 3A–3C). In addition, blocking co-stimulatory ligand CD80 alone, or together with co-stimulatory ligand CD86, diminished the generation of T_{REG} cells (Figures 3A–3C). Interestingly, the activation of non-T_{REG} cells, as addressed by the expression of CD25 and lack of FoxP3, required MHC class

II and co-stimulatory molecules but not IL-2 (Figure 3C). As programmed death-ligand 1 (PD-L1) expression by LECs has been implicated as essential for the deletional tolerance of autoreactive $CD8^+$ T cells (Tewalt et al., 2012), we also added PD-L1 blocking antibody in our co-culture. Notably, no significant effects on T_{REG} cell conversion were observed when using the PD-L1 blocking antibody (Figures 3A–3C). Several studies reported that IL-2 together with transforming growth factor β (TGF-β) has a significant effect on the induction, maintenance, and function of T_{REG} cells (Chen et al., 2003; Park et al., 2004; Zheng et al., 2007). However, TGF-β did not seem to be involved in LNSC-mediated conversion of naive $CD4^+$ T cells, as T_{REG} cells were still present when cultured together with the K14-mOva LEC line in the presence of neutralizing anti-TGF-β (Figures 3A–3C), as seen in a recent study (Akamatsu et al., 2019). These data further support an essential role of IL-2 and co-stimulatory molecules in the conversion of naive $CD4^+$ T cells into $CD25^+FoxP3^+$ T_{REG} cells upon the recognition of self-antigens, presented by LNSCs in the context of MHC class II molecules.

In accordance with these findings, low levels of MHC class II, compared to expression levels on DCs, were detected on all LNSC subsets when freshly isolated, as shown before (Baptista et al., 2014; Dubrot et al., 2018, 2014; Malhotra et al., 2012) (Figures 3D and 3E). Furthermore, CD80 was mainly expressed by FRCs and LECs derived from steady-state peripheral LNs and LNSC lines (Figures 3D, 3E, and S5A). CD86 expression was barely detectable on either freshly isolated LNSCs or cell lines, whereas PD-L1 expression was detected at low levels on some FRCs and at higher levels on endothelial cells (Figures 3D, 3E, and S5A). To further visualize the expression of MHC class II and other co-stimulatory molecules, we applied t-distributed stochastic neighbor embedding (t-SNE) unsupervised clustering (Amir et al., 2013) to the manually gated $CD45^-Ter\text{-}119^-$ LNSCs using the online analysis platform Cytobank (Figures S5B and S5C for gating strategy). The tSNE maps indicate the existence of LNSCs, particularly FRCs, that co-expressed MHC class II and co-stimulatory molecules at low levels, making them suitable as antigen-presenting stromal cells involved in converting the naive $CD4^+$ T cells into T_{REG} cells (Figure 3F). Altogether, these results indicate that steady-state LNSCs express low levels of MHC class II and co-stimulatory molecules, which are required for the conversion of naive $CD4^+$ T cells into T_{REG} cells in an IL-2 dependent manner.

LNSCs Control Autoreactive T_{FH} Cells

As T_{FH} cells are known to be important players in establishing autoimmune diseases (Craft, 2012), the potential role of LNSCs in controlling autoreactive T_{FH} cells *in vivo* was addressed by transplanting LNs of WT and K14-mOva mice into WT C57BL/6J hosts, followed by the transfer of Ova-specific TCR-transgenic naive $CD4^+$ OT-II T cells and immunization with Ova in incomplete Freund's adjuvant (IFA) for 4 and 10 days (Figure 4A). Analysis at day 4 showed a significant reduction in Ova-specific $Cxcr5^+PD1^+Bcl6^+$ T_{FH} cells (OT-II T_{FH}) within K14-mOva Tx LNs when compared to WT Tx LNs, which were no longer apparent at day 10 (Figures 4B and 4C). However, no effect on OT-II T_{FH} cells was seen within endogenous LNs in mice that received K14-mOva Tx LNs (Figures 4D and 4E). Furthermore, transplantation and immunization did not affect the endogenous pools of T_{FH} (endo-T_{FH}) and T_{REG} (endo-T_{REG}) cells (Figures S6A–S6D). The transferred OT-II T_{REG} cells were similar in frequency at day 4 after transfer in both K14-mOva and WT Tx LNs, while an increase in OT-II T_{REG} cells was seen in WT Tx LNs at day 10 (Figure S6E). The frequencies of endo-T_{FH}, endo-T_{REG}, and OT-II T_{REG} cells were not influenced in endogenous LNs (Figures S6F–S6I). Collectively, our data suggest a critical function of LNSCs in controlling the formation of autoreactive T_{FH} cells.

IL-2 Is Required for LNSC-Dependent Control of Autoreactive T_{FH} Cells

T_{REG} cells have been implicated to control antigen-specific T_{FH} cells' expansion (Wing et al., 2014). Our data suggest that the conversion of naive $CD4^+$ T cells toward T_{REG} cells controls the formation of autoreactive T_{FH} cells within LNs. To investigate this possibility, the function of T_{REG} cells was blocked by providing neutralizing IL-2 antibodies when WT Tx and K14-mOva Tx mice were immunized with Ova in IFA. Neutralizing IL-2 antibodies or an isotype control were provided daily for 4 days. Next, the fate of the transferred $CD4^+$ OT-II T cells was analyzed (Figure 5A). As expected, autoreactive OT-II T_{FH} cells were strongly reduced in K14-mOva Tx LNs, compared to WT Tx LNs, when treated with an isotype control antibody (Figures 5B and 5C). However, the frequency of autoreactive OT-II T_{FH} cells in K14-mOva Tx LNs treated with anti-IL-2 was similar to that of WT Tx LNs (Figures 5B and 5C). Importantly, both OT-II T_{REG} and endo-T_{REG} cells were considerably depleted in anti-IL-2 treated mice when compared to isotype-control-treated mice (Figures 5D and 5E). Moreover, no remarkable changes in the frequency of T_{FH} cells within $CD4^+$ OT-II T in the endogenous LNs were observed (Figures 5F and 5G). Similar to the Tx LNs, OT-II T_{REG} and endo-T_{REG} cell frequencies in the endogenous LNs were strongly reduced in anti-IL-2-treated animals when compared to isotype control animals (Figures 5H and 5I). Collectively, our data indicate that upon IL-2 blocking, T_{REG} cells no longer control the generation of T_{FH} cells that react to self-antigens expressed and presented by LNSC and are thus autoreactive.

Self-Antigen Presentation by LNSCs Controls Autoreactive B Cell Formation

Since T_{FH} cells are critical for the development and maintenance of GC B cells (Breitfeld et al., 2000; Schaerli et al., 2000; Victora and Nussenzweig, 2012; Walker et al., 1999), the formation of Ova-specific GC B cells within Tx LNs was determined. For this purpose, WT or K14-mOva LNs were transplanted into WT C57BL/6J mice, followed by an intravenous injection of Ova-specific TCR-transgenic naive $CD4^+$ OT-II T cells 4 weeks post-transplantation. After 18 h, the mice received a subcutaneous injection of Ova in IFA, and 10 days later, $CD19^+CD38^-GL7^+Ova^+$ GC B cells in Tx LNs were analyzed (Figure 6A). The frequencies of total B cells and GC B cells were comparable between Tx LNs from WT and K14-mOva mice (Figures 6B–6D). However, the Ova-specific B cells were significantly reduced in K14-mOva Tx LNs, as compared to WT Tx LNs (Figures 6B and 6E). Moreover, the reduction of

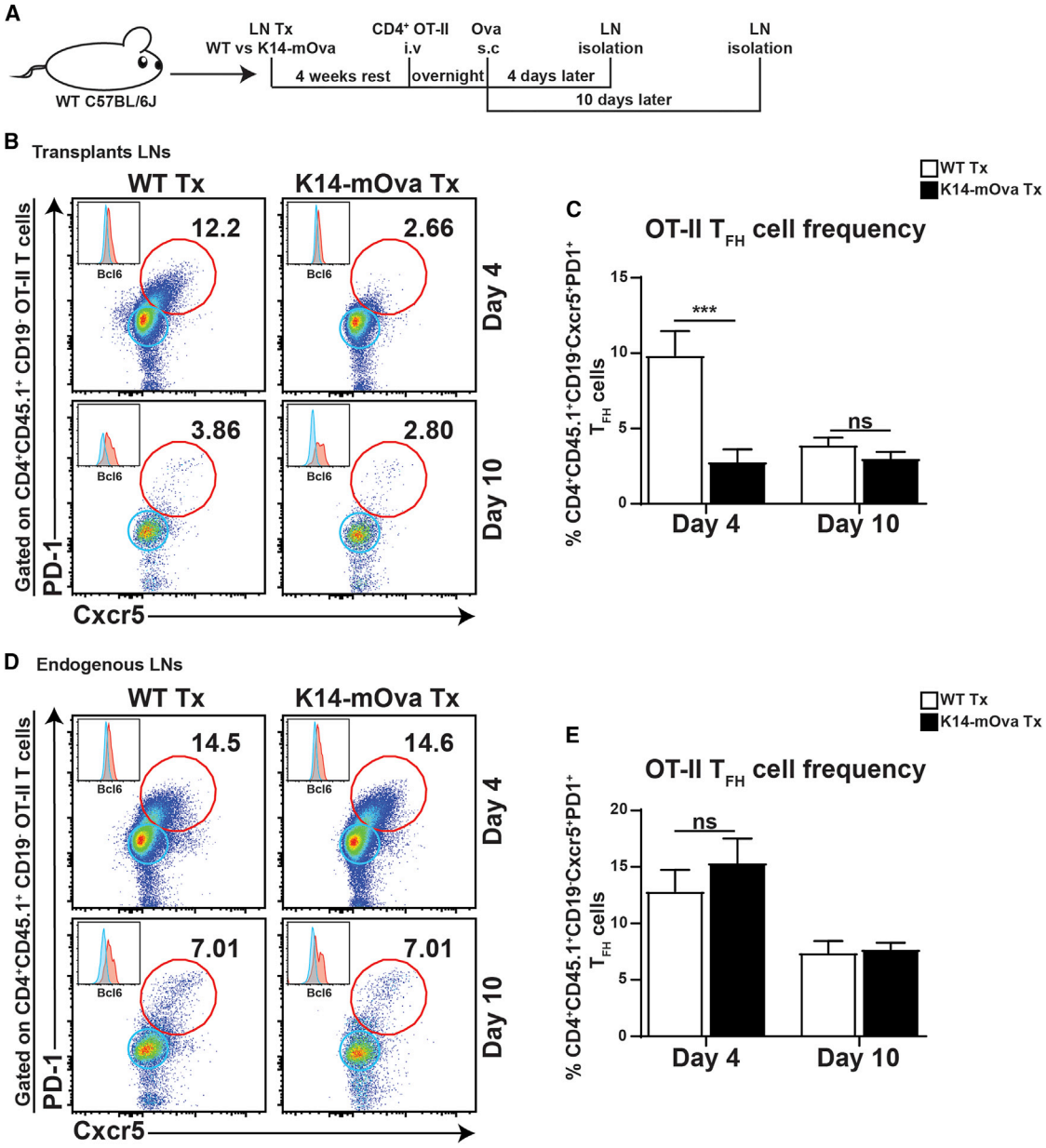

Figure 4. Formation of Autoreactive T_{FH} Cells Is Controlled by LNSCs

(A) *In vivo* experimental design to study the effect of self-antigen-presenting LNSCs on T_{FH} cell formation. WT Tx and K14-mOva Tx mice were intravenously injected with 10×10^6 transgenic CD45.1$^+$CD4$^+$ OT-II T cells. After 18 h, mice were injected with Ova/IFA in the ankles of both hind legs. 4 days and 10 days later, mice were sacrificed, transferred CD45.1$^+$CD4$^+$ OT-II T cells were transplanted, and endogenous LNs were examined using flow cytometry.

(B and D) Representative density plots of CD45.1$^+$CD4$^+$CD19$^-$ OT-II T cells are shown. The numbers in the plots display the percentage of Cxcr5$^+$PD-1$^+$ T_{FH} (OT-II T_{FH}) cells of all live CD45.1$^+$CD4$^+$ T cells within (B) the transplanted and (D) the endogenous LNs. Histograms represent the expression of Bcl6 in Cxcr5$^-$PD-1$^-$ (blue; non-T_{FH}) and Cxcr5$^+$PD-1$^+$ (red; T_{FH}) T cells within the live CD45.1$^+$CD4$^+$ T cell population.

(C and E) The graphs represent the percentage of OT-II T_{FH} cells of all live CD45.1$^+$CD4$^+$ T cells within (C) the transplanted and (E) the endogenous LNs. Data show the mean ± SEM of a combination of two independent experiments for day 4 (WT Tx, n = 10 mice; K14-mOva Tx, n = 10 mice in total) and one independent experiment for day 10 (WT Tx, n = 5 mice; K14-mOva Tx, n = 5 mice in total). Statistical analyses were done by two-way ANOVA followed by Turkey's multiple comparison test. ***$p < 0.001$; ns, not significant.

Ova-specific B cells was restricted to K14-mOva Tx LNs, as the endogenous LNs showed similar frequencies of B cells, GC B cells, and Ova-specific GC B cells (Figures 6F–6I). Altogether, these results support a model in which self-antigen-presenting LNSCs promote the differentiation of autoreactive CD4$^+$ T cells into T_{REG} cells while preventing the generation of T_{FH} cells, thereby reducing GC B cells' formation directed against the same self-antigen.

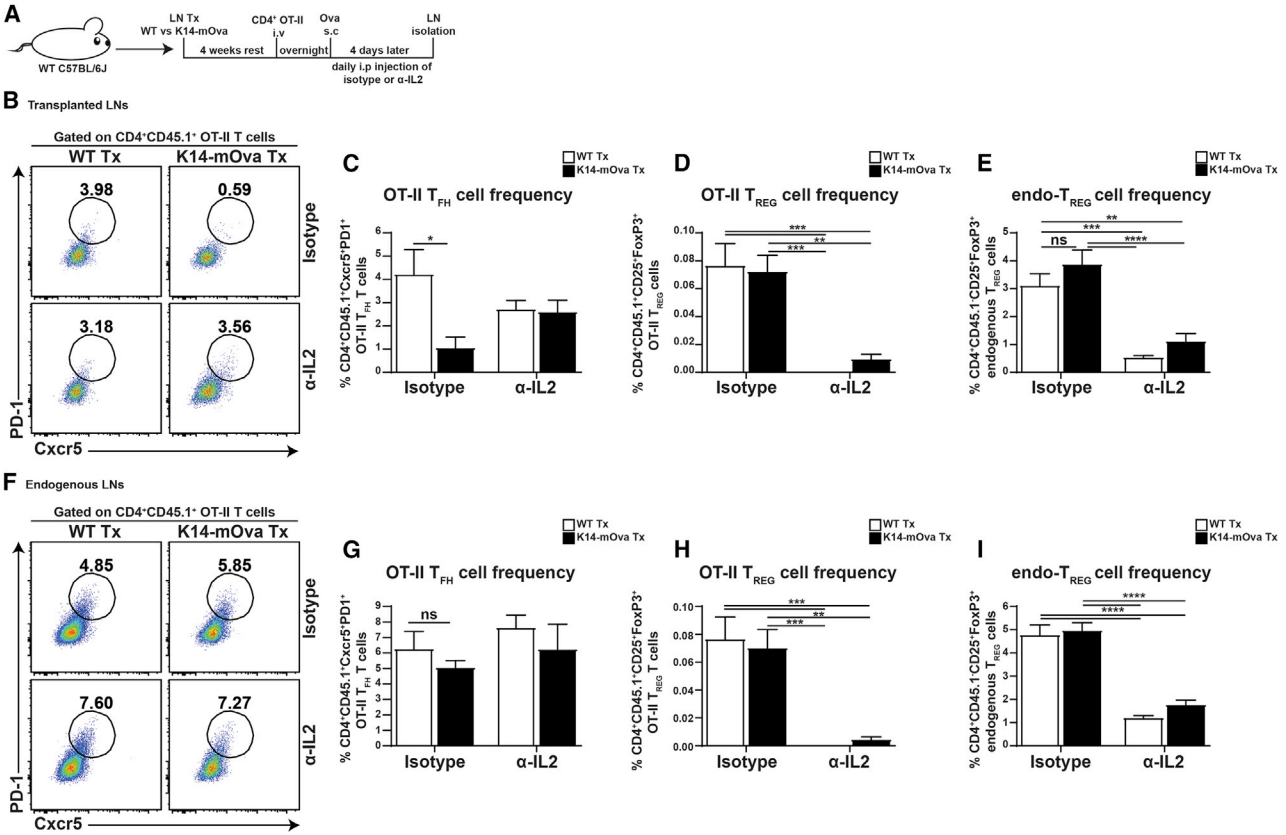

Figure 5. Blockade of IL-2 *In Vivo* Prevents T_{REG} Development and Favors Autoreactive T_{FH} Cell Formation

(A) *In vivo* experimental design to study the role of IL-2 in LNSC-mediated T_{FH} cell suppression. WT Tx and K14-mOva Tx mice were intravenously injected with 10×10^6 transgenic CD45.1$^+$CD4$^+$ OT-II T cells. After 18 h, mice were injected with Ova/IFA in the ankles of both hind legs. Mice were injected intraperitoneally with isotype control or anti-IL2-neutralizing antibodies once a day for 4 days. At day 5, mice were sacrificed, and transferred CD45.1$^+$CD4$^+$ OT-II T cells in both transplanted and endogenous LNs were examined using flow cytometry.

(B and F) Representative density plots of live CD45.1$^+$CD4$^+$Cxcr5$^+$PD-1$^+$ T_{FH} cells are shown. The numbers in the plot display the frequency of Cxcr5$^+$PD-1$^+$ T_{FH} cells within the live CD45.1$^+$CD4$^+$ T cell population of (B) the transplanted and (F) the endogenous LNs.

(C and G) The graphs represent the frequency of OT-II Cxcr5$^+$PD-1$^+$ T_{FH} (OT-II T_{FH}) cells within the live CD45.1$^+$CD4$^+$ T cell population of the (C) transplanted and (G) endogenous LNs.

(D, E, H, and I) The graphs represent the frequency of (D and H) CD45.1$^+$CD4$^+$CD25$^+$FoxP3$^+$ OT-II T_{REG} cells and (E and I) CD45.1$^-$CD4$^+$CD25$^+$FoxP3$^+$ endogenous (endo) T_{REG} cells within the live CD4$^+$ T cell population of the (D and E) transplanted and (H and I) endogenous LNs. Data shown are the mean ± SEM (WT Tx, n = 6 mice; K14-mOva Tx, n = 6 mice) and are representative of two independent experiments. Statistical analyses were done by two-way ANOVA followed by Turkey's multiple comparison test. *p < 0.05; **p < 0.001; ***p < 0.0001; ****p < 0.0001; ns, not significant.

DISCUSSION

The repertoires of naive T cells as well as T_{REG} cells are generated in the thymus, and after completion of their thymic differentiation, naive T cells enter the periphery. Through the expression of LN homing receptors, naive T cells migrate with great efficiency to the LNs, where they may encounter the antigen that they can specifically recognize with their TCR when presented by hematopoietic antigen-presenting cells. This migration is also important for the interaction with LNSCs to complete the control of autoreactive T cell development (Dubrot et al., 2014; Lee et al., 2007; Magnusson et al., 2008; Rouhani et al., 2015; Tewalt et al., 2012). Our data showed that the presentation of self-antigens in the context of MHC class II molecules by LNSCs, together with the assistance of DCs, resulted in the conversion of naive CD4$^+$ T cells into T_{REG} cells. Furthermore, the converted T_{REG} cells were methylated to a similar degree as seen in naive CD4$^+$ T cells, unlike the demethylated TSDR in thymic T_{REG} cells, providing further evidence that the converted cells are derived from naive T cells. These T_{REG} cells lacked Cxcr5 and PD-1 expression, which are classical markers of T_{FH} cells, suggesting that converted T_{REG} cells do not have follicular regulatory T cell (Tfr) properties (Fonseca et al., 2019; Sage and Sharpe, 2016), at least at day 3 after T cell transfer. This conversion was antigen specific and required CD80 co-stimulation, as well as IL-2. Both LECs and FRCs have the capacity to mediate this conversion *in vitro*, while converted T_{REG} cells are preferentially found within the T cell zone close to the B cell follicles at 3 days after the T cell transfer. Since FRCs, as well as LECs, can be found around the B cell follicles, both populations may be responsible for this process within our system (Cohen et al., 2014). Blocking the function of T_{REG} cells by anti-IL-2 allowed the development of antigen-specific T_{FH} cells.

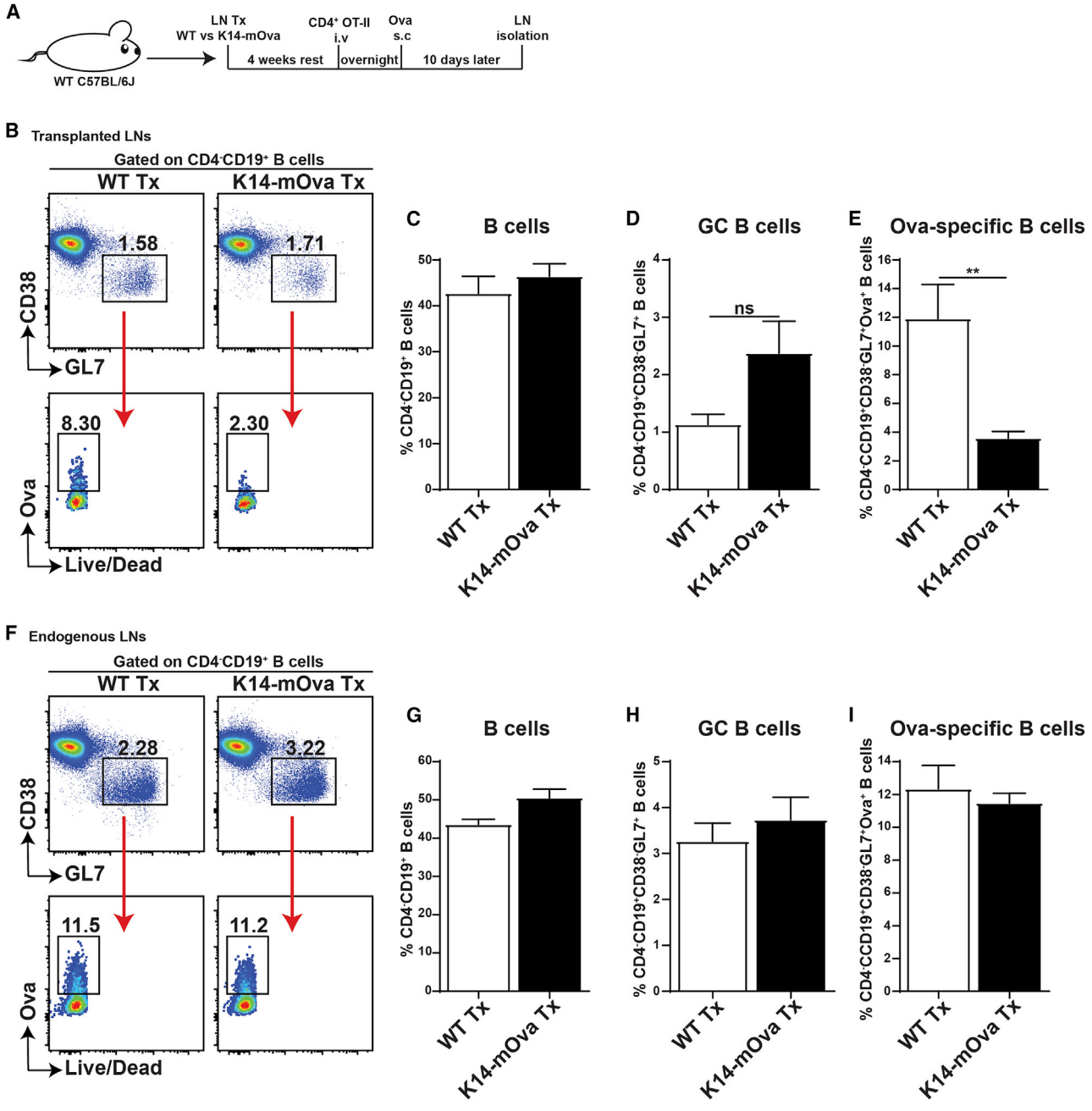

Figure 6. LNSCs Control the Formation of Autoreactive GC B Cells

(A) *In vivo* experimental design to study the effect of self-antigen-presenting LNSCs on GC B cell formation. WT Tx and K14-mOva Tx mice were intravenously injected with 10×10^6 transgenic CD45.1$^+$CD4$^+$ OT-II T cells. After 18 h, mice were injected subcutaneously with Ova/IFA in the ankles of both hind legs. 10 days later, mice were sacrificed, and B cells in both transplanted and endogenous LNs were examined using flow cytometry.

(B and F) Representative density plots of CD4$^-$CD19$^+$ B cells are shown. The numbers in the top plots display the frequency of CD38$^-$GL7$^+$ GC B cells, and bottom plots display Ova$^+$ B cells within the live CD4$^-$CD19$^+$CD38$^-$GL7$^+$ GCs B cell population of (B) the transplanted and (F) the endogenous LNs.

(C–E and H–I) The graphs represent the frequencies of (C and G) CD4$^-$CD19$^+$ B cells, (D and H) CD38$^-$GL7$^+$ GC B cells, and (E and I) Ova$^+$-specific GC B cells within the live CD4$^-$CD19$^+$ B cell population of the transplanted and endogenous LNs. Data shown represent the mean ± SEM (n = 5 mice per group) and are representative of two independent experiments. Data are analyzed by unpaired Student's t test. **$p < 0.001$; ns, not significant.

Our data indicate that LNSCs can inhibit the development of autoreactive B cells by promoting T_{REG} cell formation at the expense of T_{FH} cells' generation from autoreactive CD4$^+$ T cells.

Analysis of freshly isolated LNSCs showed that both FRCs and LECs expressed low levels of MHC class II and co-stimulatory CD80, thereby marking both subsets as potential

antigen-presenting LNSCs involved in the conversion of naive T cells into T_{REG} cells. In our model, Ova expression was confined to the peripheral LNSCs, as other antigen-presenting cells such as B cells, macrophages, or DCs lacked Ova expression. While both DCs and LNSCs could be the source of co-stimulatory cells, LNSCs are the obligatory source of self-antigens in the context of MHC class II molecules (Baptista et al., 2014; Dubrot et al., 2018). We propose that DCs may assist in this process, as DCs have the capacity to pick up antigen from other cells (Koble and Kyewski, 2009) and can thus participate in presenting self-antigen derived from LNSCs, leading to T cell conversion. In our transplantation model, tissue necrosis may result in such an uptake of self-antigens by DCs, leading to the conversion of endogenous Ova-specific T cells toward T_{REG} cells. Self-antigen presentation by LNSCs, when assisted by DCs, induced CD25 expression on naive $CD4^+$ T cells, suggesting an initial activation of T cells upon encountering MHC class II/peptide and CD80, potentially leading to low levels of IL-2 production. Indeed, blockade of MHC class II prevented the induction of CD25 expression, as well as the induction of FoxP3 expression. The produced levels of IL-2 were not sufficient to induce T cell proliferation (Baptista et al., 2014) but were necessary to induce the conversion of naive $CD4^+$ T cells into $CD25^+FoxP3^+$ T_{REG} cells in our *in vitro* and *in vivo* models. These results are in agreement with the essential role of IL-2 as a central player in the development, maintenance, and function of T_{REG} cells (Bayer et al., 2005; Cheng et al., 2011; D'Cruz and Klein, 2005; Fontenot et al., 2005; Malek and Bayer, 2004).

The site within the LN where converted T cells preferentially locate is within the T cell area close to the boundary of the B cell follicles. Supporting the possibility that conversion is taking place at this location is the report that clusters of pStat5-expressing $FoxP3^+$ T cells with few IL-2 producing $CD4^+$ T cells are present within LNs in steady state at the outer T cell areas close to the B cell follicles. This specific localization required TCR triggering, suggesting antigen encounter by T cells at the B-T cell border (Liu et al., 2015). It is therefore likely that within this area subsets of sessile LNSCs that present self-antigens are localized. The recently described population of $CCL19^{lo}$ LNSCs is specifically assigned to reside within this area at the T-B cell border. Interestingly, these cells potentially co-express the necessary molecules MHC class II and CD80 (Rodda et al., 2018). Furthermore, $CCL19^{lo}$ LNSCs express all molecules required to attract immune cells to such regulatory hotspots, as mRNA transcripts for CCL21 and Ch25h—described to attract DCs as well as B and T cells—are detected in these cells (Rodda et al., 2018). These locations could be the same as those in which conventional DC2 (cDC2), a DC subset, together with naive $CD4^+$ T cells were described to localize, promoting $CD4^+$ T cell help for $CD8^+$ T cell responses (Baptista et al., 2019). Thus, by attracting incoming naive T cells to these self-antigen-presenting stromal cells, autoreactive T cells can be converted into T_{REG} cells and come into contact with DCs in order to further control potential autoreactive T cells.

The subclass of IL-2-producing $CD4^+$ T cells that were shown to be present in steady-state LNs was not further specified (Liu et al., 2015). However, a recent report by DiToro et al. (2018) showed IL-2-producing T cells to be precursors for T_{FH} cells. Thus, autoreactive naive $CD4^+$ T cells that have not been depleted in the thymus and reach peripheral LNs can differentiate into T_{FH} cells upon self-antigen encounter, thereby providing IL-2 for the generation of T_{REG} cells, as we show here. When access to self-antigen recognition is denied, larger quantities of IL-2 are produced and clustering of $pStat5^+$ cells is lost, leading to the loss of control of T effector cells by T_{REG} cells (Liu et al., 2015). Similarly, within our experiments, blockade of T_{REG} cells resulted in an increase in T_{FH} cells. As these T_{FH} cells were directed against self-antigen expressed by LNSCs, we could follow the consequences of these autoreactive T_{FH} cells for the differentiation of antigen-specific B cells. Indeed, increased numbers of T_{FH} cells resulted in an increase in B cells specific for the same antigen. Thus, our data strongly suggest that the generation of autoreactive B and T cells can be controlled at the level of LNSCs, and dysregulation of LNSCs (e.g., as a result of an ongoing infection) may result in autoantibody production, leading to autoimmunity. Interestingly, we have shown that human LNSCs are functionally altered during the earliest phases of rheumatoid arthritis (Hähnlein et al., 2018a, 2018b), potentially allowing unwanted activation of autoreactive lymphocytes. Since elevated levels of T_{FH} cells and B cells are seen in patients that are at high risk of a broad range of autoimmune diseases (Crotty, 2014; Gensous et al., 2018; van Baarsen et al., 2013), these observations are also clinically relevant.

In conclusion, our *in vitro* and *in vivo* data show the existence of a unique population of LNSCs that express MHC class II and possess co-stimulatory properties in steady state. Thereby, with the support of DCs, they provide essential signals to naive $CD4^+$ T cells to facilitate the generation of antigen-specific T_{REG} cells in an IL-2-dependent manner. By doing so, LNSCs limit autoreactive T_{FH} cell formation and control the autoreactive humoral immune response. The function of these LNSCs need to be further studied in humans during health and autoimmunity to explore whether we can use their properties for therapeutic strategies.

STAR★METHODS

Detailed methods are provided in the online version of this paper and include the following:

- KEY RESOURCES TABLE
- LEAD CONTACT AND MATERIALS AVAILABILITY
- EXPERIMENTAL MODEL AND SUBJECT DETAILS
  - Mice
- METHOD DETAILS
  - LN transplantation
  - Adoptive transfer
  - Immunization
  - IL-2 neutralization
  - Flow cytometry
  - Immunofluorescence staining
  - LNSC lines preparation
  - T cell co-culture assays
  - Quantitative RT-PCR
  - Methylation analysis of the TSDR
- QUANTIFICATION AND STATISTICAL ANALYSIS
  - Statistical analysis
- DATA AND CODE AVAILABILITY

SUPPLEMENTAL INFORMATION

Supplemental Information can be found online at https://doi.org/10.1016/j.celrep.2020.03.007.

ACKNOWLEDGMENTS

We thank M.M.J. van Gool, M.N. Erkelens, A.C. Breedveld, A.V. Bos, T. Smeekes, I. Licht, and H. van der Laan for excellent technical support. This work was financially supported by grants from ReumaFonds (14-2-403 to R.E.M.), NWO-ALW (ALWOP.271 to J.J.K.), and NWO-ZonMW (VENI 916.13.011 to R.M.R.; VIDI 917183711 to L.G.M.v.B.; TOP 01217014 to R.E.M. and L.G.M.v.B.).

AUTHOR CONTRIBUTIONS

R.N. and R.E.M. designed the experiments, discussed the data, and wrote the manuscript. R.N., C.G.d.G., E.D.K., J.J.K., S.d.K., T.K., and R.M.R. performed the experiments. S.H., J.B., L.G.M.v.B., and R.M.R. revised the manuscript.

DECLARATION OF INTERESTS

The authors declare no competing interests.

Received: November 7, 2019
Revised: January 13, 2020
Accepted: February 28, 2020
Published: March 24, 2020

REFERENCES

Abbas, A.K., Trotta, E., R Simeonov, D., Marson, A., and Bluestone, J.A. (2018). Revisiting IL-2: Biology and therapeutic prospects. Sci. Immunol. *3*, eaat1482.

Akamatsu, M., Mikami, N., Ohkura, N., Kawakami, R., Kitagawa, Y., Sugimoto, A., Hirota, K., Nakamura, N., Ujihara, S., Kurosaki, T., et al. (2019). Conversion of antigen-specific effector/memory T cells into Foxp3-expressing T_{reg} cells by inhibition of CDK8/19. Sci. Immunol. *4*, eaaw2707.

Amir, el-A.D., Davis, K.L., Tadmor, M.D., Simonds, E.F., Levine, J.H., Bendall, S.C., Shenfeld, D.K., Krishnaswamy, S., Nolan, G.P., and Pe'er, D. (2013). viSNE enables visualization of high dimensional single-cell data and reveals phenotypic heterogeneity of leukemia. Nat. Biotechnol. *31*, 545–552.

Anderson, M.S., Venanzi, E.S., Klein, L., Chen, Z., Berzins, S.P., Turley, S.J., von Boehmer, H., Bronson, R., Dierich, A., Benoist, C., and Mathis, D. (2002). Projection of an immunological self shadow within the thymus by the aire protein. Science *298*, 1395–1401.

Arroyo-Villa, I., Bautista-Caro, M.B., Balsa, A., Aguado-Acín, P., Bonilla-Hernán, M.G., Plasencia, C., Villalba, A., Nuño, L., Puig-Kröger, A., Martín-Mola, E., and Miranda-Carús, M.E. (2014). Constitutively altered frequencies of circulating follicullar helper T cell counterparts and their subsets in rheumatoid arthritis. Arthritis Res. Ther. *16*, 500.

Aschenbrenner, K., D'Cruz, L.M., Vollmann, E.H., Hinterberger, M., Emmerich, J., Swee, L.K., Rolink, A., and Klein, L. (2007). Selection of Foxp3+ regulatory T cells specific for self antigen expressed and presented by Aire+ medullary thymic epithelial cells. Nat. Immunol. *8*, 351–358.

Baptista, A.P., Roozendaal, R., Reijmers, R.M., Koning, J.J., Unger, W.W., Greuter, M., Keuning, E.D., Molenaar, R., Goverse, G., Sneeboer, M.M., et al. (2014). Lymph node stromal cells constrain immunity via MHC class II self-antigen presentation. eLife *3*.

Baptista, A.P., Gola, A., Huang, Y., Milanez-Almeida, P., Torabi-Parizi, P., Urban, J.F., Jr., Shapiro, V.S., Gerner, M.Y., and Germain, R.N. (2019). The Chemoattractant Receptor Ebi2 Drives Intranodal Naive CD4(+) T Cell Peripheralization to Promote Effective Adaptive Immunity. Immunity *50*, 1188–1201.e1186.

Baron, U., Floess, S., Wieczorek, G., Baumann, K., Grützkau, A., Dong, J., Thiel, A., Boeld, T.J., Hoffmann, P., Edinger, M., et al. (2007). DNA demethylation in the human FOXP3 locus discriminates regulatory T cells from activated FOXP3(+) conventional T cells. Eur. J. Immunol. *37*, 2378–2389.

Bayer, A.L., Yu, A., Adeegbe, D., and Malek, T.R. (2005). Essential role for interleukin-2 for CD4(+)CD25(+) T regulatory cell development during the neonatal period. J. Exp. Med. *201*, 769–777.

Bianchi, T., Pincus, L.B., Wurbel, M.A., Rich, B.E., Kupper, T.S., Fuhlbrigge, R.C., and Boes, M. (2009). Maintenance of peripheral tolerance through controlled tissue homing of antigen-specific T cells in K14-mOVA mice. J. Immunol. *182*, 4665–4674.

Breitfeld, D., Ohl, L., Kremmer, E., Ellwart, J., Sallusto, F., Lipp, M., and Förster, R. (2000). Follicular B helper T cells express CXC chemokine receptor 5, localize to B cell follicles, and support immunoglobulin production. J. Exp. Med. *192*, 1545–1552.

Chen, W., Jin, W., Hardegen, N., Lei, K.J., Li, L., Marinos, N., McGrady, G., and Wahl, S.M. (2003). Conversion of peripheral CD4+CD25- naive T cells to CD4+CD25+ regulatory T cells by TGF-beta induction of transcription factor Foxp3. J. Exp. Med. *198*, 1875–1886.

Cheng, G., Yu, A., and Malek, T.R. (2011). T-cell tolerance and the multi-functional role of IL-2R signaling in T-regulatory cells. Immunol. Rev. *241*, 63–76.

Cohen, J.N., Guidi, C.J., Tewalt, E.F., Qiao, H., Rouhani, S.J., Ruddell, A., Farr, A.G., Tung, K.S., and Engelhard, V.H. (2010). Lymph node-resident lymphatic endothelial cells mediate peripheral tolerance via Aire-independent direct antigen presentation. J. Exp. Med. *207*, 681–688.

Cohen, J.N., Tewalt, E.F., Rouhani, S.J., Buonomo, E.L., Bruce, A.N., Xu, X., Bekiranov, S., Fu, Y.X., and Engelhard, V.H. (2014). Tolerogenic properties of lymphatic endothelial cells are controlled by the lymph node microenvironment. PLoS ONE *9*, e87740.

Craft, J.E. (2012). Follicular helper T cells in immunity and systemic autoimmunity. Nat. Rev. Rheumatol. *8*, 337–347.

Crotty, S. (2014). T follicular helper cell differentiation, function, and roles in disease. Immunity *41*, 529–542.

Cuadrado, E., van den Biggelaar, M., de Kivit, S., Chen, Y.Y., Slot, M., Doubal, I., Meijer, A., van Lier, R.A.W., Borst, J., and Amsen, D. (2018).). Proteomic Analyses of Human Regulatory T Cells Reveal Adaptations in Signaling Pathways that Protect Cellular Identity. Immunity *48*, 1046–1059.e1046.

D'Cruz, L.M., and Klein, L. (2005). Development and function of agonist-induced CD25+Foxp3+ regulatory T cells in the absence of interleukin 2 signaling. Nat. Immunol. *6*, 1152–1159.

Derbinski, J., Schulte, A., Kyewski, B., and Klein, L. (2001). Promiscuous gene expression in medullary thymic epithelial cells mirrors the peripheral self. Nat. Immunol. *2*, 1032–1039.

DiToro, D., Winstead, C.J., Pham, D., Witte, S., Andargachew, R., Singer, J.R., Wilson, C.G., Zindl, C.L., Luther, R.J., Silberger, D.J., et al. (2018). Differential IL-2 expression defines developmental fates of follicular versus nonfollicular helper T cells. Science *361*, eaao2933.

Dubrot, J., Duraes, F.V., Potin, L., Capotosti, F., Brighouse, D., Suter, T., LeibundGut-Landmann, S., Garbi, N., Reith, W., Swartz, M.A., and Hugues, S. (2014). Lymph node stromal cells acquire peptide-MHCII complexes from dendritic cells and induce antigen-specific $CD4^+$ T cell tolerance. J. Exp. Med. *211*, 1153–1166.

Dubrot, J., Duraes, F.V., Harlé, G., Schlaeppi, A., Brighouse, D., Madelon, N., Göpfert, C., Stokar-Regenscheit, N., Acha-Orbea, H., Reith, W., et al. (2018). Absence of MHC-II expression by lymph node stromal cells results in autoimmunity. Life Sci. Alliance *1*, e201800164.

Fletcher, A.L., Lukacs-Kornek, V., Reynoso, E.D., Pinner, S.E., Bellemare-Pelletier, A., Curry, M.S., Collier, A.R., Boyd, R.L., and Turley, S.J. (2010). Lymph node fibroblastic reticular cells directly present peripheral tissue antigen under steady-state and inflammatory conditions. J. Exp. Med. *207*, 689–697.

Fletcher, A.L., Malhotra, D., Acton, S.E., Lukacs-Kornek, V., Bellemare-Pelletier, A., Curry, M., Armant, M., and Turley, S.J. (2011). Reproducible isolation of

lymph node stromal cells reveals site-dependent differences in fibroblastic reticular cells. Front. Immunol. *2*, 35.

Floess, S., Freyer, J., Siewert, C., Baron, U., Olek, S., Polansky, J., Schlawe, K., Chang, H.D., Bopp, T., Schmitt, E., et al. (2007). Epigenetic control of the foxp3 locus in regulatory T cells. PLoS Biol. *5*, e38.

Fonseca, V.R., Ribeiro, F., and Graca, L. (2019). T follicular regulatory (Tfr) cells: Dissecting the complexity of Tfr-cell compartments. Immunol. Rev. *288*, 112–127.

Fontenot, J.D., Rasmussen, J.P., Gavin, M.A., and Rudensky, A.Y. (2005). A function for interleukin 2 in Foxp3-expressing regulatory T cells. Nat. Immunol. *6*, 1142–1151.

Gensous, N., Charrier, M., Duluc, D., Contin-Bordes, C., Truchetet, M.E., Lazaro, E., Duffau, P., Blanco, P., and Richez, C. (2018). T Follicular Helper Cells in Autoimmune Disorders. Front. Immunol. *9*, 1637.

Hähnlein, J.S., Nadafi, R., de Jong, T., Ramwadhdoebe, T.H., Semmelink, J.F., Maijer, K.I., Zijlstra, I.A., Maas, M., Gerlag, D.M., Geijtenbeek, T.B.H., et al. (2018a). Impaired lymph node stromal cell function during the earliest phases of rheumatoid arthritis. Arthritis Res. Ther. *20*, 35.

Hähnlein, J.S., Ramwadhdoebe, T.H., Semmelink, J.F., Choi, I.Y., Berger, F.H., Maas, M., Gerlag, D.M., Tak, P.P., Geijtenbeek, T.B.H., and van Baarsen, L.G.M. (2018b). Distinctive expression of T cell guiding molecules in human autoimmune lymph node stromal cells upon TLR3 triggering. Sci. Rep. *8*, 1736.

Hammerschmidt, S.I., Ahrendt, M., Bode, U., Wahl, B., Kremmer, E., Förster, R., and Pabst, O. (2008). Stromal mesenteric lymph node cells are essential for the generation of gut-homing T cells in vivo. J. Exp. Med. *205*, 2483–2490.

He, J., Tsai, L.M., Leong, Y.A., Hu, X., Ma, C.S., Chevalier, N., Sun, X., Vandenberg, K., Rockman, S., Ding, Y., et al. (2013). Circulating precursor CCR7(lo) PD-1(hi) CXCR5^{+} CD4^{+} T cells indicate Tfh cell activity and promote antibody responses upon antigen reexposure. Immunity *39*, 770–781.

Hinterberger, M., Aichinger, M., Prazeres da Costa, O., Voehringer, D., Hoffmann, R., and Klein, L. (2010). Autonomous role of medullary thymic epithelial cells in central CD4(+) T cell tolerance. Nat. Immunol. *11*, 512–519.

Jordan, M.S., Boesteanu, A., Reed, A.J., Petrone, A.L., Holenbeck, A.E., Lerman, M.A., Naji, A., and Caton, A.J. (2001). Thymic selection of CD4+CD25+ regulatory T cells induced by an agonist self-peptide. Nat. Immunol. *2*, 301–306.

Josefowicz, S.Z., Lu, L.F., and Rudensky, A.Y. (2012). Regulatory T cells: mechanisms of differentiation and function. Annu. Rev. Immunol. *30*, 531–564.

Koble, C., and Kyewski, B. (2009). The thymic medulla: a unique microenvironment for intercellular self-antigen transfer. J. Exp. Med. *206*, 1505–1513.

Lee, J.W., Epardaud, M., Sun, J., Becker, J.E., Cheng, A.C., Yonekura, A.R., Heath, J.K., and Turley, S.J. (2007). Peripheral antigen display by lymph node stroma promotes T cell tolerance to intestinal self. Nat. Immunol. *8*, 181–190.

Li, L.C., and Dahiya, R. (2002). MethPrimer: designing primers for methylation PCRs. Bioinformatics *18*, 1427–1431.

Liu, Z., Gerner, M.Y., Van Panhuys, N., Levine, A.G., Rudensky, A.Y., and Germain, R.N. (2015). Immune homeostasis enforced by co-localized effector and regulatory T cells. Nature *528*, 225–230.

Ma, J., Zhu, C., Ma, B., Tian, J., Baidoo, S.E., Mao, C., Wu, W., Chen, J., Tong, J., Yang, M., et al. (2012). Increased frequency of circulating follicular helper T cells in patients with rheumatoid arthritis. Clin. Dev. Immunol. *2012*, 827480.

Magnusson, F.C., Liblau, R.S., von Boehmer, H., Pittet, M.J., Lee, J.W., Turley, S.J., and Khazaie, K. (2008). Direct presentation of antigen by lymph node stromal cells protects against CD8 T-cell-mediated intestinal autoimmunity. Gastroenterology *134*, 1028–1037.

Malek, T.R., and Bayer, A.L. (2004). Tolerance, not immunity, crucially depends on IL-2. Nat. Rev. Immunol. *4*, 665–674.

Malek, T.R., Yu, A., Vincek, V., Scibelli, P., and Kong, L. (2002). CD4 regulatory T cells prevent lethal autoimmunity in IL-2Rbeta-deficient mice. Implications for the nonredundant function of IL-2. Immunity *17*, 167–178.

Malhotra, D., Fletcher, A.L., Astarita, J., Lukacs-Kornek, V., Tayalia, P., Gonzalez, S.F., Elpek, K.G., Chang, S.K., Knoblich, K., Hemler, M.E., et al.; Immunological Genome Project Consortium (2012). Transcriptional profiling of stroma from inflamed and resting lymph nodes defines immunological hallmarks. Nat. Immunol. *13*, 499–510.

Mebius, R.E., Brevé, J., Kraal, G., and Streeter, P.R. (1993). Developmental regulation of vascular addressin expression: a possible role for site-associated environments. Int. Immunol. *5*, 443–449.

Molenaar, R., Greuter, M., van der Marel, A.P., Roozendaal, R., Martin, S.F., Edele, F., Huehn, J., Förster, R., O'Toole, T., Jansen, W., et al. (2009). Lymph node stromal cells support dendritic cell-induced gut-homing of T cells. J. Immunol. *183*, 6395–6402.

Morita, R., Schmitt, N., Bentebibel, S.E., Ranganathan, R., Bourdery, L., Zurawski, G., Foucat, E., Dullaers, M., Oh, S., Sabzghabaei, N., et al. (2011). Human blood CXCR5(+)CD4(+) T cells are counterparts of T follicular cells and contain specific subsets that differentially support antibody secretion. Immunity *34*, 108–121.

Nichols, L.A., Chen, Y., Colella, T.A., Bennett, C.L., Clausen, B.E., and Engelhard, V.H. (2007). Deletional self-tolerance to a melanocyte/melanoma antigen derived from tyrosinase is mediated by a radio-resistant cell in peripheral and mesenteric lymph nodes. J. Immunol. *179*, 993–1003.

Owen, D.L., Mahmud, S.A., Sjaastad, L.E., Williams, J.B., Spanier, J.A., Simeonov, D.R., Ruscher, R., Huang, W., Proekt, I., Miller, C.N., et al. (2019). Thymic regulatory T cells arise via two distinct developmental programs. Nat. Immunol. *20*, 195–205.

Park, H.B., Paik, D.J., Jang, E., Hong, S., and Youn, J. (2004). Acquisition of anergic and suppressive activities in transforming growth factor-beta-costimulated CD4+CD25- T cells. Int. Immunol. *16*, 1203–1213.

Quah, B.J., Warren, H.S., and Parish, C.R. (2007). Monitoring lymphocyte proliferation in vitro and in vivo with the intracellular fluorescent dye carboxyfluorescein diacetate succinimidyl ester. Nat. Protoc. *2*, 2049–2056.

Rao, D.A., Gurish, M.F., Marshall, J.L., Slowikowski, K., Fonseka, C.Y., Liu, Y., Donlin, L.T., Henderson, L.A., Wei, K., Mizoguchi, F., et al. (2017). Pathologically expanded peripheral T helper cell subset drives B cells in rheumatoid arthritis. Nature *542*, 110–114.

Rodda, L.B., Lu, E., Bennett, M.L., Sokol, C.L., Wang, X., Luther, S.A., Barres, B.A., Luster, A.D., Ye, C.J., and Cyster, J.G. (2018). Single-Cell RNA Sequencing of Lymph Node Stromal Cells Reveals Niche-Associated Heterogeneity. Immunity *48*, 1014–1028.e1016.

Rouhani, S.J., Eccles, J.D., Riccardi, P., Peske, J.D., Tewalt, E.F., Cohen, J.N., Liblau, R., Mäkinen, T., and Engelhard, V.H. (2015). Roles of lymphatic endothelial cells expressing peripheral tissue antigens in CD4 T-cell tolerance induction. Nat. Commun. *6*, 6771.

Sage, P.T., and Sharpe, A.H. (2016). T follicular regulatory cells. Immunol. Rev. *271*, 246–259.

Schaerli, P., Willimann, K., Lang, A.B., Lipp, M., Loetscher, P., and Moser, B. (2000). CXC chemokine receptor 5 expression defines follicular homing T cells with B cell helper function. J. Exp. Med. *192*, 1553–1562.

Simpson, N., Gatenby, P.A., Wilson, A., Malik, S., Fulcher, D.A., Tangye, S.G., Manku, H., Vyse, T.J., Roncador, G., Huttley, G.A., et al. (2010). Expansion of circulating T cells resembling follicular helper T cells is a fixed phenotype that identifies a subset of severe systemic lupus erythematosus. Arthritis Rheum. *62*, 234–244.

Szabo, K., Papp, G., Barath, S., Gyimesi, E., Szanto, A., and Zeher, M. (2013). Follicular helper T cells may play an important role in the severity of primary Sjögren's syndrome. Clin. Immunol. *147*, 95–104.

Tewalt, E.F., Cohen, J.N., Rouhani, S.J., Guidi, C.J., Qiao, H., Fahl, S.P., Conaway, M.R., Bender, T.P., Tung, K.S., Vella, A.T., et al. (2012). Lymphatic endothelial cells induce tolerance via PD-L1 and lack of costimulation leading to high-level PD-1 expression on CD8 T cells. Blood *120*, 4772–4782.

van Baarsen, L.G., de Hair, M.J., Ramwadhdoebe, T.H., Zijlstra, I.J., Maas, M., Gerlag, D.M., and Tak, P.P. (2013). The cellular composition of lymph nodes in the earliest phase of inflammatory arthritis. Ann. Rheum. Dis. *72*, 1420–1424.

Victora, G.D., and Nussenzweig, M.C. (2012). Germinal centers. Annu. Rev. Immunol. *30*, 429–457.

Walker, L.S., Gulbranson-Judge, A., Flynn, S., Brocker, T., Raykundalia, C., Goodall, M., Förster, R., Lipp, M., and Lane, P. (1999). Compromised OX40 function in CD28-deficient mice is linked with failure to develop CXC chemokine receptor 5-positive CD4 cells and germinal centers. J. Exp. Med. *190*, 1115–1122.

Wang, J., Shan, Y., Jiang, Z., Feng, J., Li, C., Ma, L., and Jiang, Y. (2013). High frequencies of activated B cells and T follicular helper cells are correlated with disease activity in patients with new-onset rheumatoid arthritis. Clin. Exp. Immunol. *174*, 212–220.

Wing, J.B., Ise, W., Kurosaki, T., and Sakaguchi, S. (2014). Regulatory T cells control antigen-specific expansion of Tfh cell number and humoral immune responses via the coreceptor CTLA-4. Immunity *41*, 1013–1025.

Wolvers, D.A., Coenen-de Roo, C.J., Mebius, R.E., van der Cammen, M.J., Tirion, F., Miltenburg, A.M., and Kraal, G. (1999). Intranasally induced immunological tolerance is determined by characteristics of the draining lymph nodes: studies with OVA and human cartilage gp-39. J. Immunol. *162*, 1994–1998.

Yanaba, K., Bouaziz, J.D., Matsushita, T., Magro, C.M., St Clair, E.W., and Tedder, T.F. (2008). B-lymphocyte contributions to human autoimmune disease. Immunol. Rev. *223*, 284–299.

Zelenay, S., Lopes-Carvalho, T., Caramalho, I., Moraes-Fontes, M.F., Rebelo, M., and Demengeot, J. (2005). Foxp3+ CD25- CD4 T cells constitute a reservoir of committed regulatory cells that regain CD25 expression upon homeostatic expansion. Proc. Natl. Acad. Sci. USA *102*, 4091–4096.

Zhang, Y., Li, Y., Lv, T.T., Yin, Z.J., and Wang, X.B. (2015). Elevated circulating Th17 and follicular helper CD4(+) T cells in patients with rheumatoid arthritis. APMIS *123*, 659–666.

Zheng, S.G., Wang, J., Wang, P., Gray, J.D., and Horwitz, D.A. (2007). IL-2 is essential for TGF-beta to convert naive CD4+CD25- cells to CD25+Foxp3+ regulatory T cells and for expansion of these cells. J. Immunol. *178*, 2018–2027.

STAR★METHODS

KEY RESOURCES TABLE

REAGENT or RESOURCE	SOURCE	IDENTIFIER
Antibodies		
Anti-mouse CD45.1-eFlour 450	ThermoFisher	Cat #48-0453-82; RRID:AB_1272189
Anti-mouse CD4-Brilliant violet 786	BD-Biosciences	Cat #563331; RRID:AB_2738140
Anti-mouse CD4-Brilliant violet 785	BioLegend	Cat #100453; RRID:AB_2565843
Anti-mouse Cxcr5-Brilliant violet 605	BioLegend	Cat #145513; RRID:AB_2562208
Anti-mouse PD-1-PE-Cyanine7	ThermoFisher	Cat #25-9985-82; RRID:AB_10853805
Anti-mouse FoxP3-PE	ThermoFisher	Cat #12-5773-82; RRID:AB_465936
Anti-mouse Bcl-6-Alexa fluor 647	BD-Biosciences	Cat #561525; RRID:AB_10898007
Anti-mouse CD25-Alexa fluor 700	BioLegend	Cat #102024; RRID:AB_493709
Anti-mouse CD25-Alexa fluor 488	ThermoFisher	Cat #53-0251-82; RRID:AB_763472
Anti-mouse CD45-Pacific Blue	ThermoFisher	Cat #MCD4528; RRID:AB_10373710
Anti-mouse CD19- PE-Cyanine7	BioLegend	Cat #25-0193-82 RRID:AB_657663
Anti-mouse CD38-PE	BioLegend	Cat #102708; RRID:AB_312929
Anti-mouse GL7-Percp/cy5.5	BioLegend	Cat #144610; RRID:AB_2562979
Anti-mouse CD31-PE-Cyanine7	ThermoFisher	Cat #25-0311-82; RRID:AB_2716949
Anti-mouse GP38 (PDPN)-Alexa fluor 488	BioLegend	Cat #127406; RRID:AB_2161930
Anti-mouse CD80 (B7-1)-PE-Cyanine5	ThermoFisher	Cat #15-0801-82; RRID:AB_468774
Anti-mouse CD86 (B7-2)-PE	ThermoFisher	Cat #12-0861-82; RRID:AB_465765
Anti-mouse CD247 (PDL-1)-Pe/dazzle 594	BioLegend	Cat #124324; RRID:AB_2565639
Anti-mouse MHC-II-Alexa fluor 647	MO2Ab facility	Cat # N/A; Clone:M5/114
Anti-mouse CD11c-Alexa fluor 700	BioLegend	Cat #117320; RRID:AB_528736
Anti-mouse CD11c-eFluor 450	ThermoFisher	Cat #48-0114-82; RRID:AB_1548654
Anti-mouse CD3-PE-Cyanine7	ThermoFisher	Cat #25-0031-82; RRID:AB_469572
Anti-mouse CD11b-PE	ThermoFisher	Cat #12-0112-82; RRID:AB_2734869
Anti-mouse CD62L-Brilliant violet 711	BioLegend	Cat #104445; RRID:AB_2564215
Anti-mouse TER-119-Brilliant violet 605	BioLegend	Cat #116239; RRID:AB_2562447
Anti-mouse CD4-Alexa fluor 555	MO2Ab facility	Cat #N/A; Clone:GK1.5
Anti-mouse B220-Alexa fluor 700	BioLegend	Cat #103232; RRID:AB_493717
Anti-mouse FoxP3-eFlour 615	ThermoFisher	Cat #42-5773-82; RRID:AB_10804396
Anti-mouse Sytox blue-Alexa fluor 405	ThermoFisher	Cat #S11348
Anti-mouse IL-2	BioXcell	Cat #BE0043-1; RRID:AB_1107705
Anti-mouse IL-2	BioXcell	Cat #BE0043 RRID:AB_1107702
Anti-mouse MHC-II	BioXcell	Cat #BE0108; RRID:AB_10949298
Anti-mouse PD-L1	BioXcell	Cat #BE0101; RRID:AB_10949073
Anti-mouse CD80	BioXcell	Cat #BE0024; RRID:AB_1107676
Anti-mouse CD86	BioXcell	Cat #BE0025; RRID:AB_1107678
Anti-mouse TGF-β	BioXcell	Cat #BE0057; RRID:AB_1107757
Chemicals, Peptides, and Recombinant Proteins		
Collagenase P	Sigma-Aldrich	Cat #11213857001
Dispase II	Sigma-Aldrich	Cat #04942078001
DNase I	Sigma-Aldrich	Cat #11284932001
Collagen from calf skin	Sigma-Aldrich	Cat #C9791-50MG
Trizol	Sigma-Aldrich	Cat #15596018
Freund's Adjuvant, Incomplete	Sigma-Aldrich	F5506-10ML

(*Continued on next page*)

Continued

REAGENT or RESOURCE	SOURCE	IDENTIFIER
Critical Commercial Assays		
Fixable viability dye	ThermoFisher	Cat #65-0865-14
MagniSort mouse CD4+ T cell enrichment kit	ThermoFisher	Cat #8804-6821-74; RRID:AB_2575263
CFSE	ThermoFisher	Cat #C1157
Ovalbumin, Alexa Fluor 488 Conjugate	ThermoFisher	Cat #O34781
Ovalbumin	CalBiochem	Cat #32467 Lot #B76074-1
Intracellular Fixation and Permeabilization Buffer	ThermoFisher	Cat #00-5521-00
cDNA synthesis using RevertAid First Strand cDNA Synthesis Kit	ThermoFisher	Cat #K1622
EZ DNA Methylation-Direct kit	Zymo Research	Cat #D5021
Experimental Models: Cell Lines		
Mouse primary cell line: WT LEC	This paper	N/A
Mouse primary cell line: K14-mOva LEC	This paper	N/A
Mouse primary cell line: WT FRC	This paper	N/A
Mouse primary cell line: K14-mOva FRC	This paper	N/A
Experimental Models: Organisms/Strains		
WT C57BL/6J mice	Our colony	N/A
OT-II CD45.1	Our colony	N/A
OT-II.Rag2−/− mice	Our colony	N/A
K14-mOva mice	Our colony	N/A
Oligonucleotides		
For primers see Table S2	This paper	N/A
Software and Algorithms		
FlowJo	TreeStar Inc	https://www.flowjo.com/
Imaris	Bitplane	https://imaris.oxinst.com/
Graph Pad Prism 7	Graph Pad Software	https://www.graphpad.com/
Cytobank	Cytobank, Inc	https://www.cytobank.org/

LEAD CONTACT AND MATERIALS AVAILABILITY

Further information and requests for resources and reagents should be directed to and will be fulfilled by the Lead Contact, Reina E. Mebius (r.mebius@amsterdamumc.nl). The primary cell lines that are generated in this study have a limited lifespan and can therefore only be provided in limited numbers upon request from the Lead Contact with a completed Materials Transfer Agreement.

EXPERIMENTAL MODEL AND SUBJECT DETAILS

Mice

C57BL/6J (wild-type), human keratin 14 membrane-bound ovalbumin (K14-mOva) (on the C57BL/6 genetic background) and F1 generation of C57BL/6J-Tg (TcraTcrb) 425Cbn/J (OT-II) crossed to C57BL/6-CD45.1 (Charles River, Italy) transgenic mice were used between six to twelve weeks of age. For transplantation experiments, host and donor LNs were obtained from male mice between six to eight weeks of age. To specifically study T_{REG} cell conversion by LNSCs, we generated OT-II.Rag2$^{-/-}$ by crossing Rag2$^{-/-}$ to OT-II mice. All the mice were bred and maintained in our colony at VU university in Amsterdam. The mice were kept under specific pathogen-free conditions. All animal experiments were reviewed and approved by the VU University Scientific and Ethics Committees.

METHOD DETAILS

LN transplantation

LN transplantations were performed as described previously (Mebius et al., 1993). In brief, wild-type recipient mice were anesthetized by intraperitoneal injection of xylazine and ketamine. The popliteal fossa was chosen as the peripheral site of transplantation, after removal of the host popliteal LN. Each male recipient received two peripheral LNs (axillary, brachial or inguinal), one in each

popliteal fossa, of either wild-type or K14-mOva male donor mice. Right before transplantation, donor LNs were trimmed from surrounding fat and kept on ice in IMDM plus 10% fetal bovine serum until transplantation. Blood and lymphatic vasculatures were allowed to restore for at least 4 weeks, after which all functional experiments with transplanted LNs were performed.

Adoptive transfer

LNs and spleens of OT-II or OT-II.Rag2$^{-/-}$ transgenic mice were isolated and single cell suspensions were obtained by cutting the tissues and flushing them through a 70 μm nylon cell strainer. Splenic erythrocytes were removed with ammonium-chloride-potassium (ACK) lysis buffer for 3 min at room temperature. CD4$^+$ T cells were enriched using MagniSort mouse CD4$^+$ T cell enrichment kit (Invitrogen) following the manufacturer's instructions. Purity was on average > 85%. CFSE (Invitrogen) labeling was performed as described previously (Quah et al., 2007). 8-10x10^6 CFSE-labeled CD4$^+$ T cells were transferred intravenously (i.v.) in saline solution into the tail vein of the WT C57BL/6, K14-mOva or transplanted mice. Transplanted LNs and endogenous LNs (inguinal LNs) were isolated 4 and 10 days after injection of CD4$^+$ T cells.

Immunization

Immunization occurred the next day (around 18 hours) after adoptive transfer of CD4$^+$ OT-II T cells. Mice were immunized subcutaneously in the both ankles, with 50 μg Ova (CalBiochem), emulsified in 30% IFA (Sigma-Aldrich) in 30 μl PBS. Transplanted LNs and endogenous LNs (inguinal LNs) were isolated 4 and 10 days after immunization. Isolated lymphoid organs were passed through a 70-μm nylon cell strainer to obtain single cell suspensions for flow cytometry.

IL-2 neutralization

To examine the role of LNSCs in generating T_{REG} cell and controlling autoreactive T_{FH} cells, WT Tx and K14-mOva Tx mice were treated intraperitoneally with 0.5 mg to 1 mg of anti-IL-2 antibodies (mixture of clones JES6-1A12 and S4B6-1; BioXcell) or isotype control (2A3; BioXcell) daily for 4 days before analyzing.

Flow cytometry

Cell suspensions from LNs were stained with eBioscience Fixable Viability Dye eFluor 780 (Invitrogen) for 15 min, followed by 10 min blocking in PBS containing 5% normal mouse serum (NMS) and 2% Fetal bovine serum (FCS) (Biowest) on ice in dark. The cells were then incubated with indicated labeled antibodies (details are listed in the Key Resource Table) for 30 min in dark. For surface staining of Ova-specific B cells, cells were incubated with directly labeled Ova alexa fluor 488 (1:100, Invitrogen) for 30 min on ice in dark. For intracellular staining, cells were fixed and permeabilized for 45 min using eBioscience Intracellular Fixation and Permeabilization Buffer (Invitrogen) followed by antibody staining for intracellular molecules (details are listed in the Key Resource Table) for 60 min. Cells were washed 2 times with PBS containing 2% FCS and once with PBS before acquiring with FACS machine. All flow cytometry experiments were performed at the O2-flow facility at Amsterdam UMC, Department of Molecular Cell Biology and Immunology, using BD LSRFortessa X-20 (BD Biosciences) and analyzed with FlowJo software (TreeStar Inc.). To generate tSNE plots, the compensated live CD45$^-$Ter-119$^-$ stromal cells were exported per individual mouse into a FCS file and uploaded to the Cytobank cloud-based platform (https://www.cytobank.org/) to use visualization tools and unsupervised clustering. Using the viSNE module, we generate tSNE plots for LNSCs on the following input and analysis settings: all CD45$^-$Ter-119$^-$ stromal cells used, number of iterations: 7500, Perplexity: 30, Theta: 0.5. Cells were clustered by gp38, CD31, MHC-II, CD80, CD86 and PD-L1 expression. Next, we identified and manually gated on different subsets of LNSCs as represented by the tSNE clustering analysis color-coded, and overlaid with the expression of selected markers as represented in the graph (Figure 4D). Mean fluorescence intensity (MFI) of the indicated molecules on LNSCs and CD45$^+$CD11c$^+$ DCs were calculated using FlowJo software.

Immunofluorescence staining

LNs were dissected and fixed in 1% paraformaldehyde (PFA, Electron Microscopy Sciences) for 3 h, cryprotected in 30% sucrose (w/v) and subsequently embedded in OCT compound (Sakura Finetek Europe) and stored in −80°C until sectioning. Lymph nodes were serially sectioned (7μm) on gelatin coated slides. Sections were fixed for 10 min in acetone and blocked with blocking buffer containing 10% NMS, 1% bovine serum albumin (BSA), 0.3% Triton X-100 (Sigma-Aldrich), 0.3% tween 20 (Sigma-Aldrich) and 2% newborn calf serum (NBCS) in PBS for 1h. Sections were stained with appropriate primary and secondary antibodies (details are listed in the Key Resource Table) for 1h at room temperature and acquired using a Leica SP8 confocal microscope. Images were analyzed using Imaris Software (Bitplane, version 9.02 or higher). First, CFSE$^+$ cells were masked using the surface creation wizard including the watershed segmentation algorithm resulting in single cell objects representing individual CFSE$^+$ cells. Surface objects with FoxP3 marker expression above threshold were subsequently filtered and duplicated into new objects representing CFSE$^+$FoxP3$^+$ cells. B cell follicles were masked in a similar way using the surface creation wizard, but without cell segmentation, resulting in B cell follicle objects. Using the Imaris XT distance transformation, the shortest distance of CFSE$^+$ and CFSE$^+$FoxP3$^+$ surfaces to the outside of the B cell follicle surface was determined. These distances were exported to excel and mean distance of each cell type was calculated and used in Prism 7 (GraphPad) or higher for statistical analysis. We used Imaris snapshot function for image representations. For analysis, out of three different mice, three sections divided by at least 25 sections thus representing three different locations within each lymph node, were stained and analyzed.

LNSC lines preparation

For *in vitro* assays, skin-draining LNs (axillary, brachial and inguinal) of wild-type or K14-mOva mice were dissected, digested and sorted for long-term cultures as described before (Baptista et al., 2014; Fletcher et al., 2011). In short, skin-draining LNs were digested using the enzymatic mixture of 0.2 mg/ml collagenase P (Roche), 0.8 mg/ml Dispase II (Roche) and 0.1 mg/ml DNase I (Roche) in RPMI medium (Invitrogen) without serum. Cell suspensions were filtered through a 70-μm nylon cell strainer and then cultured on collagen (Sigma-Aldrich) coated flasks using IMDM (GIBCO) containing 10% FCS (Biowest) 2% glutamine (GIBCO) and 2% penicillin-streptomycin (GIBCO). Stromal cells were allowed to adhere to the collagen matrix and were washed after 24 h to remove non-adherent cells. After 8 days, cell cultures, primarily containing LECs and FRCs, were subsequently released from the flasks using trypsin (GIBCO), washed and sorted using BD FACSAria Fusion (BD Biosciences). The stromal cells lines were routinely characterized by flow cytometry to ensure the maintenance of stable phenotypes.

T cell co-culture assays

LNs and spleens of naive OT-II.Rag2$^{-/-}$ were dissected. Red blood cells of the spleens were lysed with ACK lysis buffer for 3 min at room temperature. Antigen-specific CD4$^+$ T cells were enriched (purity on average > 85%) using MagniSort mouse CD4$^+$ T cell enrichment kit (Invitrogen). In some experiments, CD4$^+$ T cells were sorted to 99% purity and used in co-cultures. To study the ability of LNSCs in converting naive CD4$^+$ T cells into T_{REG} cells, CD4$^+$ T cells were co-cultured with LEC and FRC cell lines derived from wild-type or K14-mOva mice at the ratio of 1:10 (stromal cell:T cell) in a 24-well plates (Greiner bio-one) for 3 to 4 days using IMDM medium (GIBCO) containing 10% FCS (Biowest) 2% glutamine (GIBCO), 2% penicillin-streptomycin (GIBCO) and 50 μM β-mercapethanol (GIBCO). In all co-cultures, stromal cells were cultured on collagen (Sigma-Aldrich) coated 24-well plates 24 h before adding the T cells. To assess the mechanism of antigen-specific T_{REG} cell conversion by LNSCs, naive CD4$^+$ T cells of OT-II.Rag2$^{-/-}$ were co-cultured with WT LECs or K14-mOva LEC in the presence of the following antibodies: anti-IL-2 (S4B6-1; 10μg/ml), anti-MHC-II (M5/114; 10μg/ml), anti-CD80 (16-10A1; 10μg/ml), anti-CD86 (GL-1; 10μg/ml), anti-PD-L1 (10F.9G2; 10μg/ml) and anti-TGF-β (1D11.16.8; 10μg/ml) for 3 days at 37°C. In some condition MHC class II restricted $Ova_{262–276}$ peptide (10 ng/ml) was added.

Quantitative RT-PCR

To evaluate self-antigens expression by LNSCs *ex vivo*, the digested LNs were pre-enriched for LNSCs using MagniSort mouse CD45$^+$ selection kit (Invitrogen). The CD45$^-$ fraction was used to sort stromal cells subsets and CD45$^+$ fraction was used to sort B cells (CD45$^+$CD19$^+$), MΦs (CD45$^+$CDIIb$^+$CDIIc$^-$) and DCs (CD45$^+$CDIIb^{int}CDIIc$^+$). For characterization of cell lines, stromal cells ($5x10^4$) were cultured on 24-well plates (Greiner bio-one) using IMDM medium (GIBCO) containing 10% FCS (Biowest) 2% glutamine (GIBCO), 2% penicillin-streptomycin (GIBCO) for 24h and washed 2 times using PBS before harvesting. For both *ex vivo* and *in vitro*, mRNA was isolated using Trizol (Invitrogen) followed by cDNA synthesis using RevertAid First Strand cDNA Synthesis Kit (Thermo Scientific) according to manufacturers' instruction. Quantitative RT-PCR was carried out using Fast SYBER™ Green Master Mix (Applied Biosystems) and ran on StepOnePlus real-time PCR system (Applied Biosystems) or Viia 7 real-time PCR system (Applied Biosystems). The expression of genes (Supplementary Table, 1) was normalized to the expression of selected housekeeping gene.

Methylation analysis of the TSDR

Cells were proteinase K digested, followed by bisulfite conversion of genomic DNA using the EZ DNA Methylation-Direct kit according to manufacturer's protocol (Zymo Research). Fixed samples were digested for 4 h at 50°C. Methylation-specific qPCR was conducted at 98°C for 10 min, 50 cycles of 98°C for 15 s and 60°C for 1 min, followed by melt curve analysis as previously described (Cuadrado et al., 2018) on a LightCycler® 480-II (Roche). Methylation and demethylation-specific primers sets are listed in Table S1. Primers were designed using MethPrimer program (Li and Dahiya, 2002). Methylation of the TSDR (%) was calculated using the following formula: $100/(1+2^{Ct[CG]-Ct[TG]})$, where Ct[CG] is defined as Ct values obtained using methylation-specific primers and Ct [TG] is defined as Ct values obtained using demethylation-specific primers.

QUANTIFICATION AND STATISTICAL ANALYSIS

Statistical analysis

Statistical analysis was performed using Prism 7 (GraphPad) or higher. Two-tailed unpaired Student's t test and two-way ANOVA followed by Tukey's multiple comparison tests were used as required. All the data is shown as mean ± SEM and p values < 0.05 were considered significant.

DATA AND CODE AVAILABILITY

This study did not generate datasets or code.

Cell Reports, Volume *30*

Supplemental Information

Lymph Node Stromal Cells Generate Antigen-Specific Regulatory T Cells and Control Autoreactive T and B Cell Responses

Reza Nadafi, Catarina Gago de Graça, Eelco D. Keuning, Jasper J. Koning, Sander de Kivit, Tanja Konijn, Sandrine Henri, Jannie Borst, Rogier M. Reijmers, Lisa G.M. van Baarsen, and Reina E. Mebius

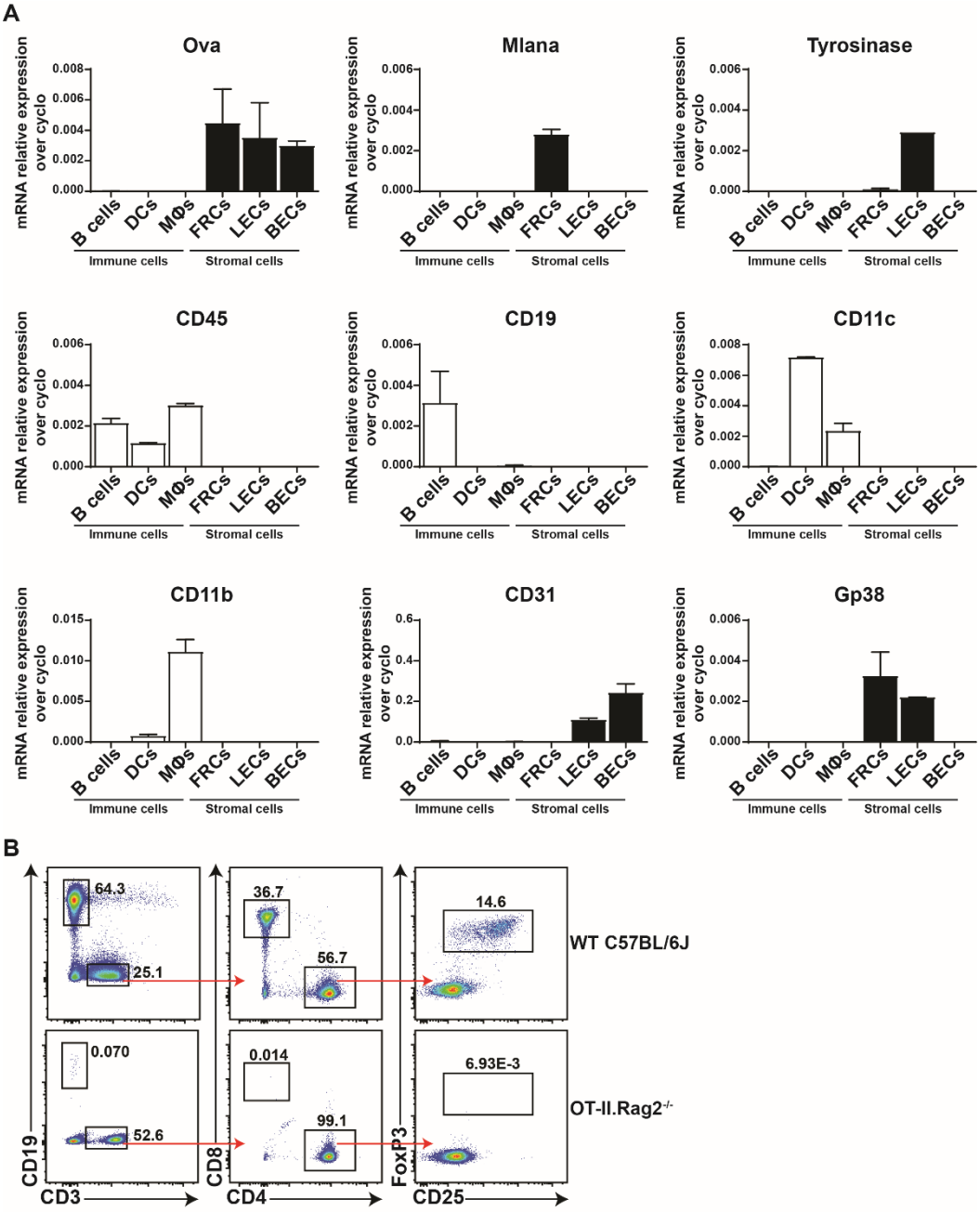

Fig. S1 related to Fig. 1. Characterization of K14-mOva and OT-II.Rag2$^{-/-}$ mice. (**A**) Self-antigen expression in K14-mOva LN is restricted to stromal cells. Peripheral LNs from K14-mOva were collected and enzymatically digested. The cell suspension were pre-enriched into CD45^{-} and CD45^{+} cells using CD45^{+} selection kit. Enriched CD45^{-} cells (negative selection) were sorted into the following subsets: FRCs (CD45^{-}CD31^{-}GP38^{+}), LECs (CD45^{-}CD31^{+}GP38^{+}) and BECs (CD45^{-}CD31^{+}GP38^{-}). Enriched CD45^{+} cells (positive selection) were sorted into the following subsets: B cells (CD45^{+}CD19^{+}CD11c^{-}CD11b^{-}), Dendritic cells (DCs) (CD45^{+}CD19^{-}CD11c^{+}CD11b^{int}) and Macrophages (MΦs) (CD45^{+}CD19^{-}CD11c^{-}CD11b^{+}). mRNA expression level of CD45, CD19, CD11c, CD11b, CD31, Gp38, Ova, Mlana and tyrosinase in cells derived from peripheral LNs of K14-mOva mice was determined by real-time qPCR. The graphs shown represent the mean ± SEM (n=2). **(B)** Spleens from WT C57BL/6J and OT-II.Rag2$^{-/-}$ were collected and erythrocytes were removed with ACK lysis buffer and stained for immune cells. Representative density plots are shown, numbers next to the drawn gates represent the frequency of CD19^{+} B cells, CD3^{+} T cells, CD8^{+} T cells, CD4^{+} T cells and CD25^{+}FoxP3^{+} T_{REG} cells within live cells. The graphs shown, represent one experiment (WT C57BL/6J, n=3; OT-II.Rag2$^{-/-}$, n=3).

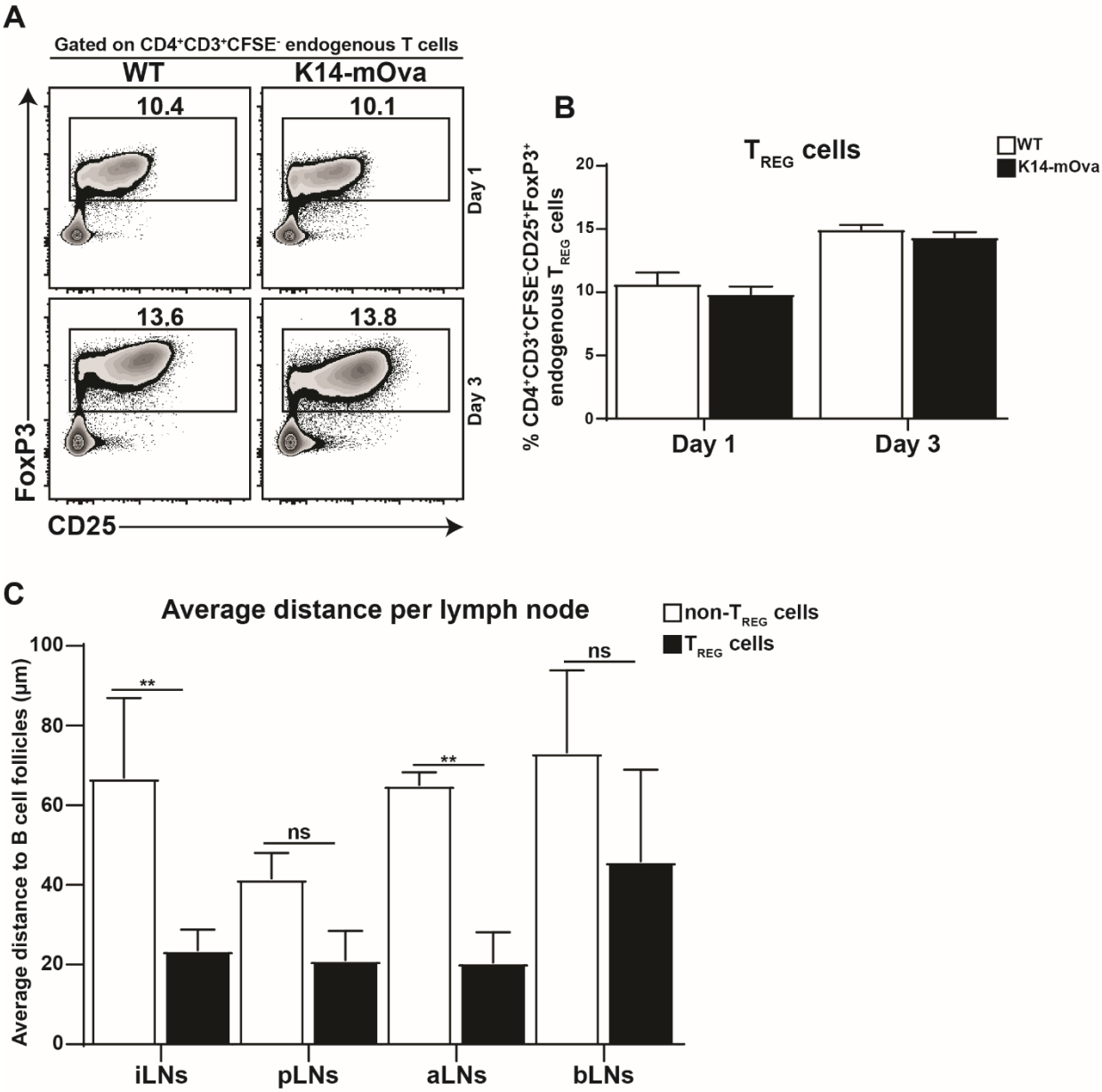

Fig. S2 related to Fig. 1. Quantification of endogenous T_{REG} and converted T_{REG} cells. (**A**) Representative contour plots of live endogenous $CD4^+CD3^+$ T cells in peripheral LNs, in which the numbers in the plots display the frequency of $CD25^+FoxP3^+$ T_{REG} cells. (**B**) Frequency of $CD25^+FoxP3^+$ T_{REG} cells within endogenous $CD4^+CD3^+$ T cells in peripheral LNs of WT and K14-mOva mice. The data in represent the mean ± SEM; one (n=4 mice per group for day 1) and two (n=3 mice per group for day 3) independent experiments. (**C**) Converted T_{REG} cells are located close to B cell area**.** Bar graph represent the average distance of $CFSE^+CD4^+FoxP3^+$ T_{REG} and $CFSE^+CD4^+FoxP3^-$ non-T_{REG} cells in indicated LNs of K14-mOva mice to the B cell area. Per mouse (n= 3) inguinal LNs (iLNs), popliteal LNs (pLNs), axillary LNs (aLNs) and brachial LNs (bLNs) were analyzed. Three sections, representing three different locations within each LN were analyzed. Data shown is the mean ± SEM (n=3). Statistical analyses were done by two-way ANOVA followed by Turkey's multiple comparison test. ***P* < 0.001, ns= not significant.

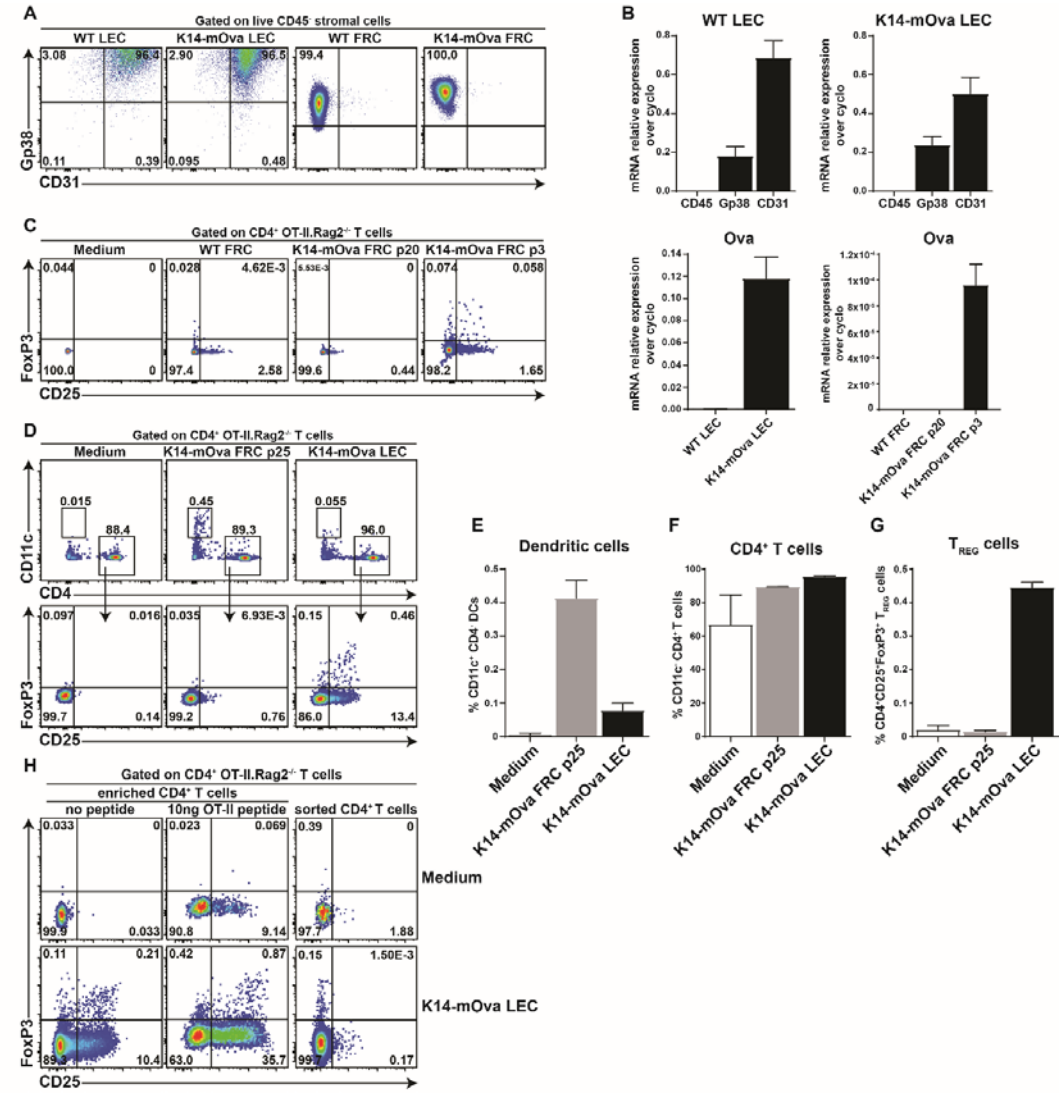

Fig. S3 related to Fig. 2. LEC and FRC mediated conversion of naïve CD4$^+$ T cells into antigen-specific T$_{REG}$ cells with assistance of dendritic cells. (**A**) Flow cytometrical characterization of the cell lines, WT LEC, K14-mOva LEC, WT FRC and K14-mOva FRC derived upon long-term culture of primary LNSCs. Representative dot plots show the expression of CD31 and Gp38 on indicated cell lines. (**B**) mRNA expression level of CD45, Gp38, CD31 and Ova in WT LEC (n=3), K14-mOva LEC (n=3), WT FRC (n=3), K14-mOva FRC passage 20 (p20) (n=3) and K14-mOva FRC p3 (n=3) cell lines was determined by real-time qPCR. The graphs shown represent the mean ± SEM. (**C**) CD4$^+$ T cells obtained from spleens of OT-II.Rag2$^{-/-}$ mice were either cultured alone (medium) (n>4) or co-incubated with WT FRC (n=3), K14-mOva FRC p20 (n=3) or K14-mOva FRC p3 (n=3) cell lines. 72 hours later, CD4$^+$ T cells were harvested and analyzed by flow cytometry. (**D**) CD4$^+$ T cells obtained from spleens of OT-II.Rag2$^{-/-}$ mice and purified by magnetic bead enrichment kit were either cultured alone (medium) (n=3) or co-cultured with K14-mOva FRC passage 25 (p25) (n=3) or K14-mOva LEC (n=3) cell lines. 72 hours later, CD4$^+$ T cells were harvested and analyzed by flow cytometry. The numbers in the upper plots display the frequency of CD11c$^+$ DCs and CD4$^+$ T cells within the live OT-II.Rag2$^{-/-}$ cells. The numbers in the lower plots display the frequency of CD25$^+$FoxP3$^+$ T$_{REG}$ cells within the live CD11c$^-$CD4$^+$ OT-II.Rag2$^{-/-}$ T cell population. The graphs represent the frequencies of (**E**) CD11c$^+$ DCs, (**F**) CD4$^+$ T cells and (**G**) CD25$^+$FoxP3$^+$ T$_{REG}$ cells within the population of enriched OT-II.Rag2$^{-/-}$ lymphocytes. The data represent the mean ± SEM. (**H**) CD4$^+$ T cells enriched using magnetic beads or sorted on live CD4$^+$ T cells (99% pure) from spleens of OT-II.Rag2$^{-/-}$ mice and were cultured alone (medium) (n=2) or co-incubated with K14-mOva LEC (n=2) cell line. MHC-II restricted OVA$_{262–276}$ peptide (10 ng/ml) was added to magnetic beads enriched CD4$^+$ T cells. Representative density plots are shown. The numbers in the plots display the frequency of CD25$^+$FoxP3$^+$ T$_{REG}$ cells in medium and K14-mOva LEC.

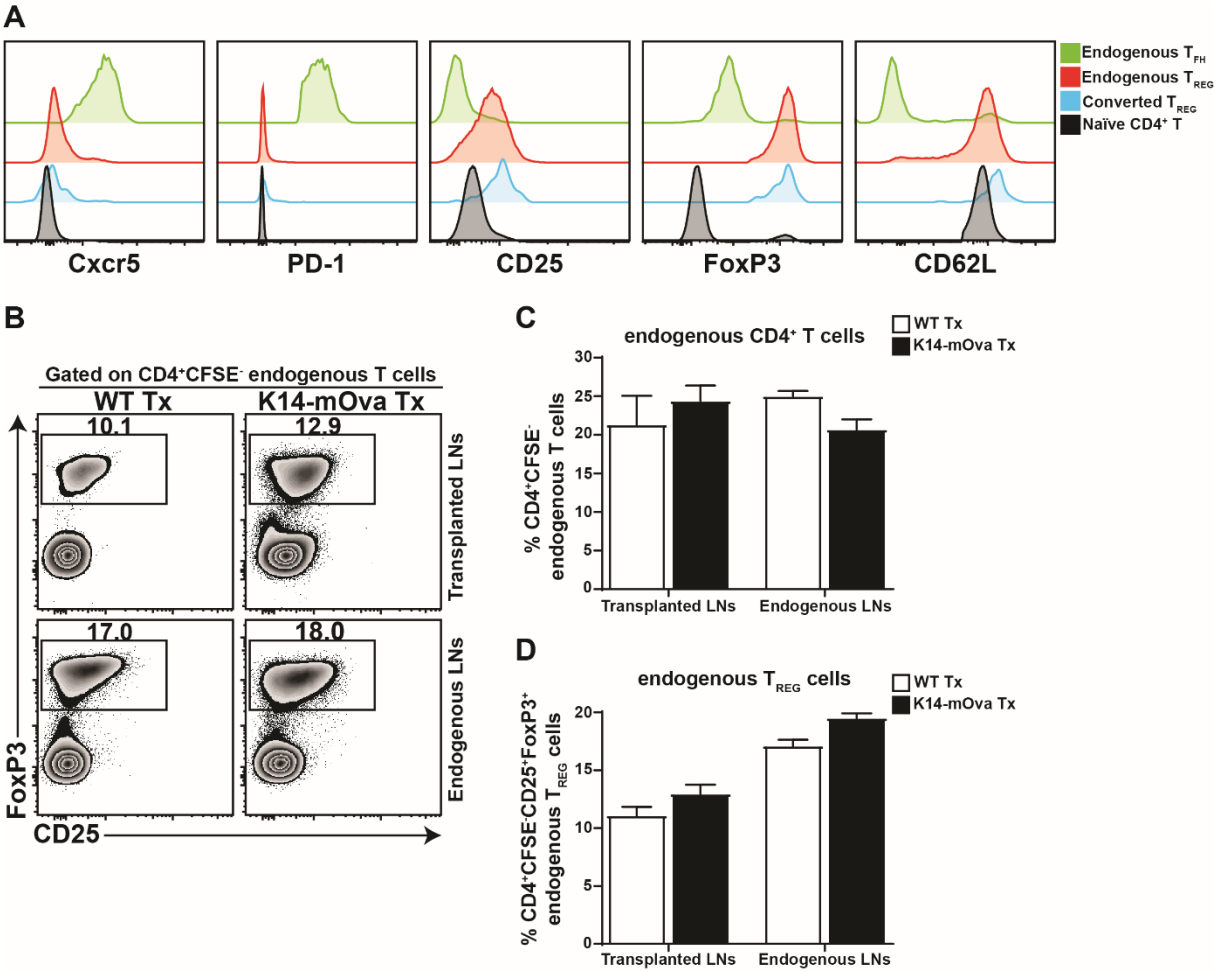

Fig. S4 related to Fig. 2. Characterization of converted CD25$^+$FoxP3$^+$ T$_{REG}$ cells and endogenous CD4$^+$ T cells in transplanted K14-mOva LNs. (A) Transplanted K14-mOva mice were intravenously injected with 8x10^6 CFSE labelled CD4$^+$ OT-II.Rag2$^{-/-}$ T cells. Four days after CD4$^+$ T cell transfer, mice were sacrificed and converted CD25$^+$FoxP3$^+$ T$_{REG}$ cells were examined using flow cytometry. Representative histograms show the expression of indicated molecules on naïve endogenous CD4$^+$ T cells (CD4$^+$CFSE$^-$CD62L$^+$), converted T$_{REG}$ (CD4$^+$CFSE$^+$CD25$^+$FoxP3$^+$), endogenous T$_{REG}$ (CD4$^+$CFSE$^-$CD25$^+$FoxP3$^+$) and endogenous T$_{FH}$ (CD4$^+$CFSE$^-$ Cxcr5$^+$PD-1$^+$) in K14-mOva transplanted LNs (n=5). (**B**) Representative contour plots of live endogenous CD4$^+$CD3$^+$ T cells in peripheral LNs, in which the numbers in the plots display the frequency of endogenous CD25$^+$FoxP3$^+$ T$_{REG}$ cells. (**C**) Frequency of endogenous CD4$^+$CD3$^+$CFSE$^-$ T cells in peripheral LNs of WT and K14-mOva mice. (**D**) Frequency of endogenous CD25$^+$FoxP3$^+$ T$_{REG}$ cells within the live CD4$^+$CD3$^+$CFSE$^-$ T cell population. Data in (C) and (D) represent the mean ± SEM; n=5 mice per group.

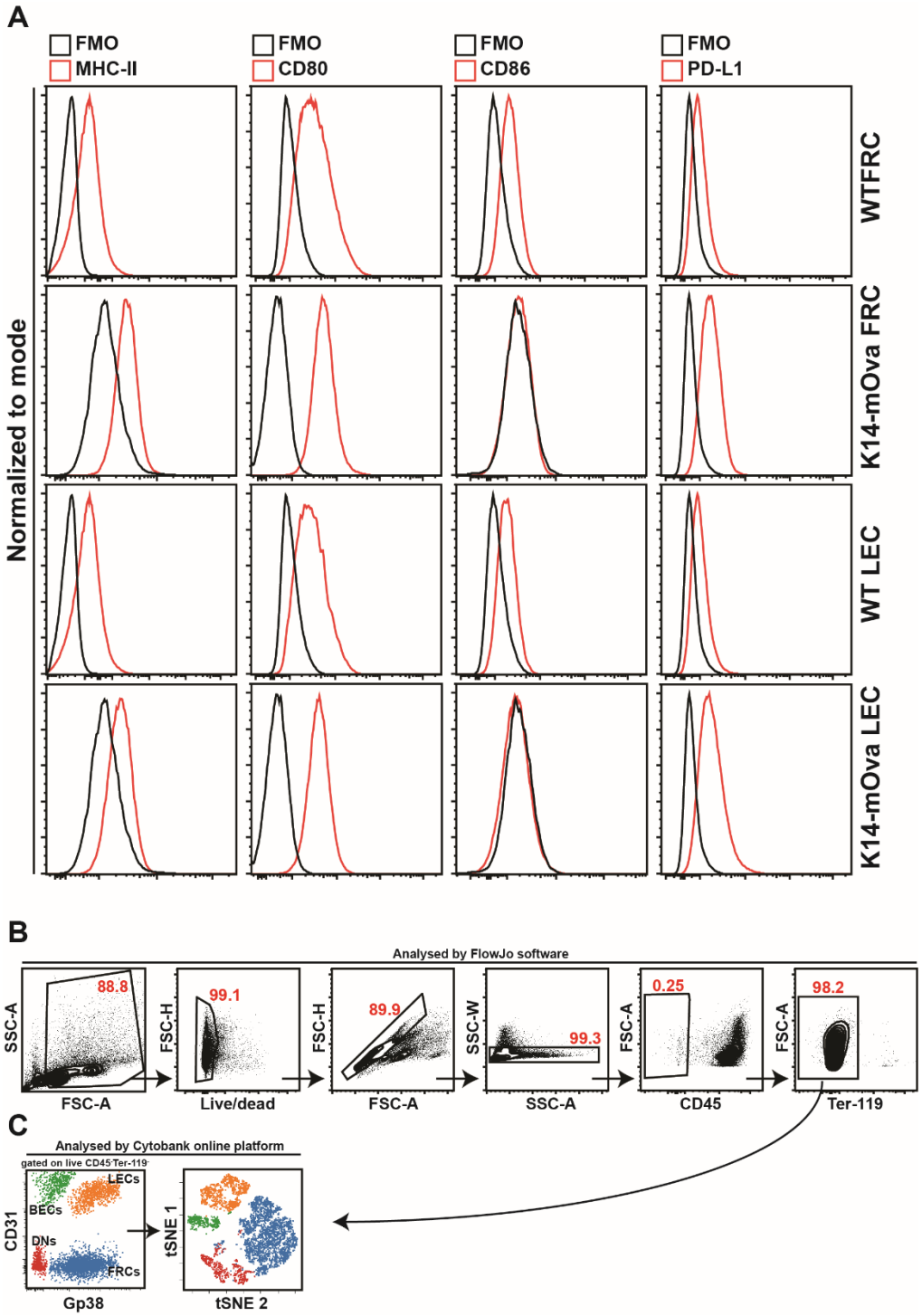

Fig. S5 related to Fig. 3. Characterization of LNSC lines and gating strategy of LNSC subsets for tSNE plots. (A) Expression of co-stimulatory and inhibitory molecules on WT FRC (n=3) and K14-mOva FRC (n=3), WT LEC (n=3) and K14-mOva LEC (n=3) cell lines was assessed using flow cytometry. (**B**) Classical gating strategy of peripheral LNSCs based on gp38 and CD31 expression. The compensated live CD45^{-}Ter-119^{-} FCS file was exported from FlowJo analysis software and analyzed using the online analysis platform Cytobank. (**C**) The plot represent high dimensional data in a two-dimensional plot (tSNE1 vs. tSNE2). Cells that are identical in expression are clustered together in space.

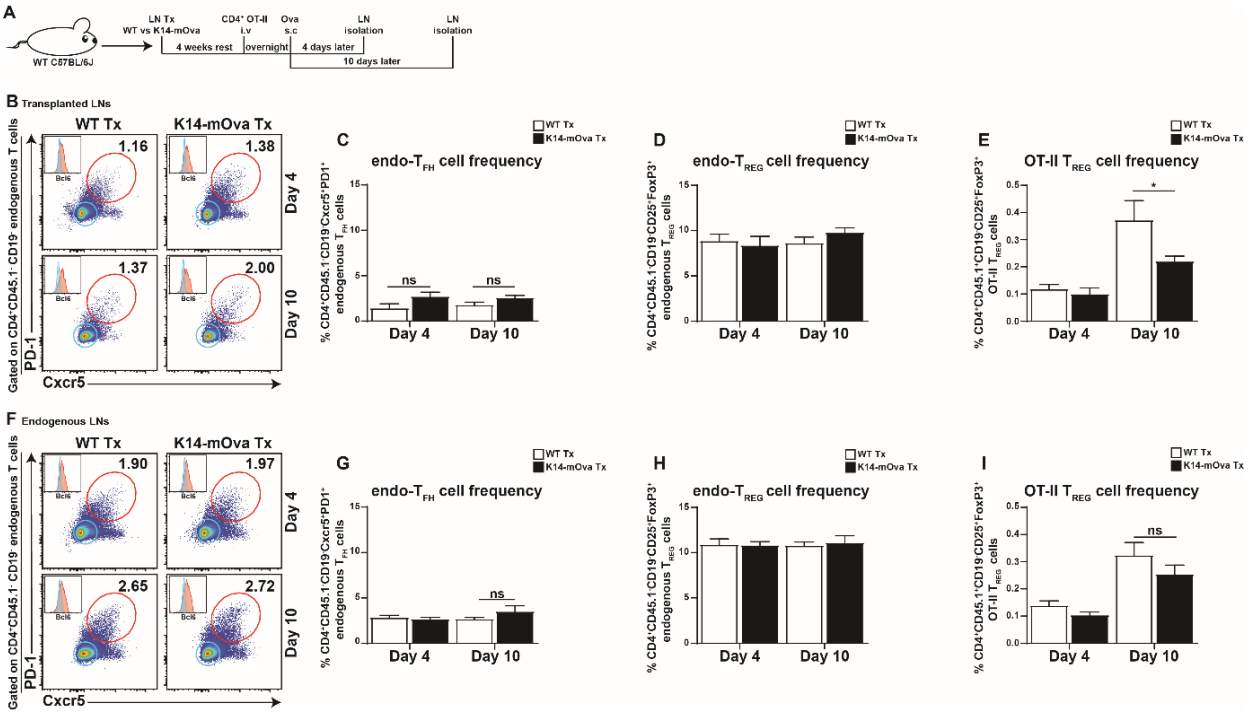

Fig. S6 related to Fig. 4. Endogenous T_{FH} and T_{REG} cells are not affected by the transplantation of K14-mOva LNs. (**A**) In vivo experimental design to study the effect of self-antigen presenting LNSCs cells on T_{FH} cell formation. WT Tx and K14-mOva Tx mice were intravenously injected with $10x10^6$ transgenic $CD45.1^+CD4^+$ OT-II T cells. 18 hours later, mice were injected with Ova/IFA in the ankles of both hind legs. 4 days and 10 days later, mice were sacrificed and endogenous $CD45.1^-CD4^+$ T cells of both transplanted and endogenous LNs were examined using flow cytometry. (**B and F**) Representative density plots of endogenous $CD45.1^-CD4^+CD19^-$ T cells are shown. The numbers in the plots display the frequency of $Cxcr5^+PD\text{-}1^+$ T_{FH} (endo-T_{FH}) cells within the live endogenous $CD45.1^-CD4^+$ T cell population of the transplanted and endogenous LNs. Histograms represent the expression of Bcl6 in $Cxcr5^-PD\text{-}1^-$ (blue) and $Cxcr5^+PD\text{-}1^+$ (red) T cells within the live endogenous $CD45.1^-CD4^+$ T cell population. (**C and G**) The graphs represent the frequency of endo-T_{FH} cells within the live endogenous $CD45.1^-CD4^+$ T cell population of the transplanted and endogenous LNs. (**D and H**) The graphs represent the frequency of $CD45.1^-CD4^+CD25^+FoxP3^+$ endogenous T_{REG} (endo-T_{REG}) and **(E and I)** $CD45.1^-CD4^+CD25^+FoxP3^+$ transferred OT-II T_{REG} cells within the live $CD4^+$ T cell population of the transplanted and endogenous LNs. Data show the mean ± SEM of a combination of 2 independent experiments for day 4 (WT Tx, n=10 mice; K14-mOva Tx, n=10 mice in total) and 1 independent experiments for day 10 (WT Tx, n=5 mice; K14-mOva Tx, n=5 mice in total). Statistical analyses were done by two-way ANOVA followed by Turkey's multiple comparison test. ns= not significant.

Related to STAR method: Supplementary Table 1. Primer sequences

Gene	Forward sequence	Reverse sequence
Cyclo	ACC CAT CAA ACC ATT CCT TCT GTA	TGA GGA AAA TAT GGA ACC CAA AGA
CD31	TGG TTG TCA TTG GAG TGG TC	TTC TCG CTG TTG GAG TTC AG
GP38	CAC CCT GGT TGG AAT CAT AGT TG	TAG GGC GAG ACC TTC CAG AAA
Ova	GCT ATG GGC ATT ACT GAC GTG	TGC TGA GGA GAT GCC AGA C
CD45	CCC CGG GAT GAG ACA GTT G	AAA GCC CGA GTG CCT TCC T
CD19	GTG CTC TCC CTT CCT ACA TC	CTG ACC TTC TTC TTC CCC TC
CD11b	CCT TCA ACA AAC CAC AGT CCC G	TCC TGT CTG CGT GCC CTC AA
CD11c	CAG AGC CAG AAC TTC CCA AC	GAC TAA CTA CCG AGC CCA TC
Mlana	AGA AAT CCC ATC AGC CCG TG	GCG GAA GTG TGA GGG AAG TT
Tyrosinase	CCA GGC TCC CAT CTT CAG C	CCT GTG AGT GGA CTG GCA AAT
Methylation-specific	GAT AGA TTA GTT ATT TTT CGG AAC GA	ACC AAA TTT TTC TAC CAT TAA CGT C
Demethylation-specific	GGA TAG ATT AGT TAT TTT TTG GAA TGA	ACC AAA TTT TTC TAC CAT TAA CAT C